GEOPHYSICAL EXPLORATION FOR BURIED KAOLIN MINERAL

NEAR

KANKARA, KATSINA PROVINCE, KADUNA STATE, NIGERIA

BY

MICHAEL EBIPA EBIFEGHA

Thesis submitted to the Ahmadu Bello University, in partial fulfillment of the requirements for the award of the degree of

MASTER OF SCIENCE IN APPLIED GEOPHYSICS

Department of Physics
Ahmadu Bello University
Zaria - Nigeria

MAY, 1977

Dedicated to the memory of my dear father Apostle Godfrey Ebifegha, and his Royal Highness Chief Justice Owen Fiebai, whose interest in Education more than anything has brought me so far.

C O N T E N T S

			Page
Declaration			i
Acknowledgement			ii
List of figures			iii
List of maps			vi
List of tables			vii
Abbreviations			viii
Abstract			ix
Chapter One		Introduction	1
	1.1	Kaolin Deposits: uses and exploitation	1
	1.2	The Kankara kaolin deposits	5
Chapter Two		Geology	8
	2.1	General geology	8
	2.2	Geology of the kaolin	10
Chapter Three		Preliminary Analysis and Field Technique	15
	3.1	Preliminary Analysis	15
	3.1.1	Resistivity	15
	3.1.2	Gravity	18
	3.1.3	Seismic	19

	3.1.4	Magnetics	19
	3.1.5	Conclusion	19
	3.2	Field Techniques	22
Chapter Four		Resistivity Survey	25
	4.1	Introduction	25
	4.2	Instrumentation	26
	4.3	Resistivity sounding ...	29
	4.3.1	Schlumberger Electric sounding	29
	4.3.2	Central electrode sounding	49
	4.3.3	Square and crossed sounding	50
	4.4	Resistivity Profilling	63
Chapter Five		Gravity Survey	80
	5.1	Gravity field methods and error evaluation	80
	5.2	Data Processing	81
	5.3	Interpretation	82
	5.4	Density measurements	87
	5.5	Mass Estimate	90
Chapter Six		Seismic Refraction Survey	92
	6.1	Instrumentation and field work	92
	6.2	Data processing	93
	6.3	Interpretation	93

Chapter Seven		General Discussion of Results, Conclusion and Recommendations	97
	7.1	Discussion of Results	97
	7.2	Limitations of the Project	101
	7.3	Conclusions	102
	7.4	Recommendations	103

References

Appendix

DECLARATION

This is to certify that the work reported on this thesis was carried out by myself in the Geophysics section, Department of Physics, Ahmadu Bello University Zaria, at Kankara, Katsina Province, Kaduna State under the supervision of Dr. D. E. Ajakaiye (Head of Physics).

The work of others is acknowledged and referenced. No part of this thesis has been submitted elsewhere for a degree or diploma.

M.E. Ebifegha

MICHAEL EBIPA EBIFEGHA

AHMADU BELLO UNIVERSITY
ZARIA

10th May, 1977
DATE:

ACKNOWLEDGEMENT

I owe a great deal to the Department of Physics, Ahmadu Bello University for supplying all the field and computational equipment. I am particularly indebted to my project supervisor and Head of Department of Physics, Dr. D. E. Ajakaiye for her invaluable advice and guidance throughout my course of study.

Most of the computer programme used in the reduction of the field data were supplied by Mr. P. J. T. Verheijen. My thanks are due to him and also to Mr. E. E. Myada and Mr. S. B. Ojo for their useful criticism and advice. I wish to express my profound gratitude to Mr. Oyeka of the geological survey for making available his unpublished report on the area. I also wish to thank Mr. Ajibade for his useful suggestions in the geology section of this report. The assistance of Mr. M. Daniyan is greatly appreciated. I gratefully acknowledge the compliance of Mr. J. A. Adedoyin and Mr. R. A. Appah on transport matters. I am deeply indebted to members of my survey team. My thanks are surely due to Dr. D. Fincham and Dr. D. B. Umaru for their unflinching support.

My course of study was financed throughout by my uncle Justice Owen Fiebai. I am specially indebted to him.

Finally I tender my unreserved apology in case of oversight.

Lists of Figures

Fig. No		Title	Page
1.1		Typical vertical section	11
3.1		Model of Schlumberger apparent resistivity curves and the equivalent geological sections	17
4.1		Electrode configurations for sounding and profiling measurements	27
4.2		Layouts of single and crossed square array	28
4.3		Apparent resistivity section for electrical soundings	32
4.4		Interpretation of VES A, curves in terms of a 3-layer model	34
4.5	(a)	Interpretation of VES B curves in terms of a 4-layer model	37
	(b)	Comparison of the VES B curves	38
4.6		Interpretation of VES C curves in terms of a 3-layer model	41
4.7		Interpretation of VES D curves in terms of a 3-layer model	43
4.8		Interpretation of VES E curves in terms of a 3-layer model	44
4.9		Interpretation of VES F and VES G curves in terms of a 3-layer model	45

4.10	Standard graph for the determination of equivalent cases when ρ_i/ρ_{i+1} (Koefoed)	47
4.11	Results of central electrode sounding at (a) location B and (b) location D	51
4.12	Square array sounding results at location B/S, and interpretation in terms of an equivalent Schlumberger sounding	56
4.13	Square and crossed square sounding results at location D/s and interpretation in terms of an equivalent Schlumberger sounding	59
4.14	Variations of (a) apparent anisotropy and (b) apparent strike with electrode spacing	61
4.15	Correlation of borehole sections with results of colinear and square array soundings	64
4.16	Apparent - resistivity profiles along traverse aP and geologic interpretation	68
4.17	Apparent - resistivity profiles along traverse (bP) and geologic interpretation	69
4.18	Apparent - resistivity profiles along traverse (cP) and geologic interpretation	71
4.19	Apparent - resistivity profiles along traverse (dP) and geologic interpretation	72

4.20	Apparent - resistivity profiles along traverse (eP and fP)	73
4.21	Apparent - resistivity profiles along traverse (gP) and geologic interpretation	75
4.22	Lateral extent of deposit derived from the 10 m Wenner profiling results	79
5.1	Bouguer Profiles along traverses 30N, 00, and 30 S	85
5.2	Bouguer Profiles along traverses 150N and 150 S	86
5.3	Density histograms	88
6.1	Traveltime curves	94

LISTS OF MAPS

Map	Title	Page
1.	Location Map of Principal known deposits of clay	3
2.	Location Map of Kankara kaolin deposits	6
3.	Geological Map of Kankara area	9
4.	Geophysical survey Map	14
5.	Apparent resistivity survey map for 10 m, 15 m and 25 m electrode separations	76
6.	Map of apparent resistivity for 10 m electrode separation	77
7.	Residual gravity Map of the Kankara kaolin deposit	83

LISTS OF TABLES

Table	Title	Page
3.1	Physical Parameters of typical rock materials in the area	20
3.2	Results of density measurements, and anticipated gravity anomalies	21
4.1	Resistivities and thicknesses of geoelectric layers (Deduced from a 3-layer interpretation)	46
4.2	Results of square (S_1, S_2 and S_3) crossed square (S x) sounding.	62

ABBREVIATIONS

N	North
S	South
E	East
W	West
WE	West - East
m	Metre
km	Kilometre
kg	Kilogram
s	Second
Ω	Ohm
ρ	Apparent resistivity
θ	Geological strike direction
φ	Electrical strike
η	Apparent anisotropy
γ	Tripotential ratio
A.I.R.	Azimuthal Inhomogeneity Ratio
A.N.C.R. ( )	Anisotropic Non-Compatibility Ratio
g.u.	Gravity Unit
V.E.S.	Vertical electrical sounding

ABSTRACT

The results of a comprehensive geophysical study on a prominent kaolin deposit near Kankara, Katsina Province, Kaduna State, Nigeria, are discussed. The most appropriate techniques and procedures to be deployed when exploring for buried kaolin mineral of sporadic occurrence are outlined.

Electrical resistivity depth probe measurements employing both colinear and square configurations were utilized. The prevailing heterogeneities and the associated gross orientational effects in the anomalous zone limit the applicability of the collinear array sounding techniques in the determination of depths to bedrock. The crossed square sounding technique, which samples apparent resistivities in four orientations, has proved the most efficient field system in the delineation of the buried kaolin mineral deposit by resistivity methods. The apparent measure of electrical strike and vertical anisotropy as a function of electrode spacing using the crossed square array technique are obtained. Results of Wenner profiling are encouraging in the detection of near surface geological structure.

The gravity methods has proved a useful tool in mirroring the anomalous zones and in the assessment of the reserves of the concealed kaolin deposits.

The top layer structure was best delineated by the seismic refraction method; bedrock topography could not however be determined successfully.

CHAPTER ONE

INTRODUCTION

The Nigerian economy is largely dependent on its abundant mineral deposits. The economic mineral deposits include petroleum, cassiterite, columbite, coal, galena, sphalerite, wolframite, zircon, tantalite, thorite, monzite, xenotine, gold, limestone, marble, clay, shale, kaolin, feld-spar, sands and gravel. Majority of these deposits are however concealed under enormous thicknesses of overburden which sometimes tend to make their exploitation uneconomic. It is therefore absolutely essential that a preliminary appraisal of the overburden-covered deposits be made ever before the commencement of mining under the overburden.

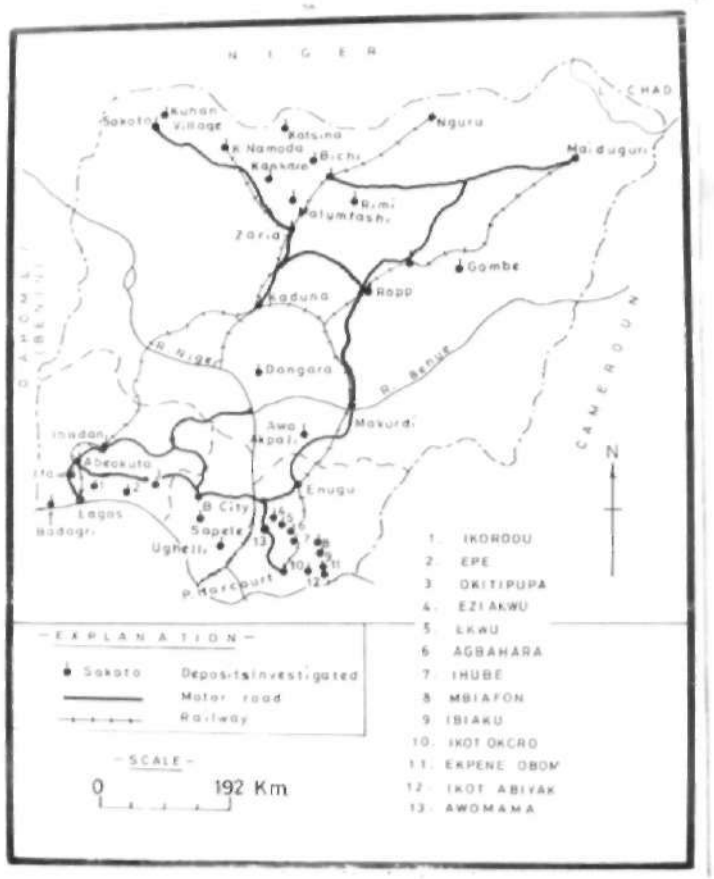
Reliable quantitative valuation of concealed potential reserves can be obtained by methods of geophysical prospecting in conjunction with geological evidence. These methods which depend on the differences in physical properties between drift and bedrock materials for their operations are easy to manipulate and relatively cheap, and are therefore supplanting other field techniques of mineral prospecting.

1.1 KAOLIN DEPOSITS: - USES AND EXPLOITATION

Kaolin is one of the naturally occuring industrial minerals of the clay family. It is distinguished from the other members primarily by its whiteness, and softness, ease of

dispersion in water and other liquids, and its negligible content of titanium and alkaline earths. (Johnstone 1961). Deposits of this mineral exploitable in commercial quantities are found only in limited areas of the country (map 1). These deposits differ greatly in appearance and constitution and have been of considerable economic importance in the Nigerian mineral industries. Among some of the products using kaolin are insecticides, paper, ceramics, fertilizers, textiles, rubber, plastics, adhesives, polishes, oilcloth, paints and cosmetics. Traditionally the mineral is also used for domestic decorations and treatment of stomach ailment.

The main mineral constituent of pure kaolin, kaolinite (Al_2O_3. 2Si O_2. $2H_2O$) is a non-magnetic and relatively good electrical conductor, having a mean relative density of 2.58 x 10^3 kg/m^3 and a fusion point of about 1,785°C (Johnstone 1961). Nkuesenam (1976) has shown a density range of 1.54 - 1.93 x 10^3 kg/m^3 for impure kaolin. These unique properties in conjunction with the contrasting physical states of most host rocks render the kaolin deposits feasible to geophysical methods of prospecting. These techniques would yield reliable information about the position, structure, quality and estimates of the reserves of the deposits. For a causative body of complicated geometry which is often the case with kaolin deposits, even extensive drilling may fail



Map I: Location map of principal known deposits of clay and Kaolin in Nigeria (compiled partly from G.M.S. 1294 KT/27/2073).

to provide adequate information of the reserves involved, and under these circumstances recourse can be made to geophysical methods of prospecting.

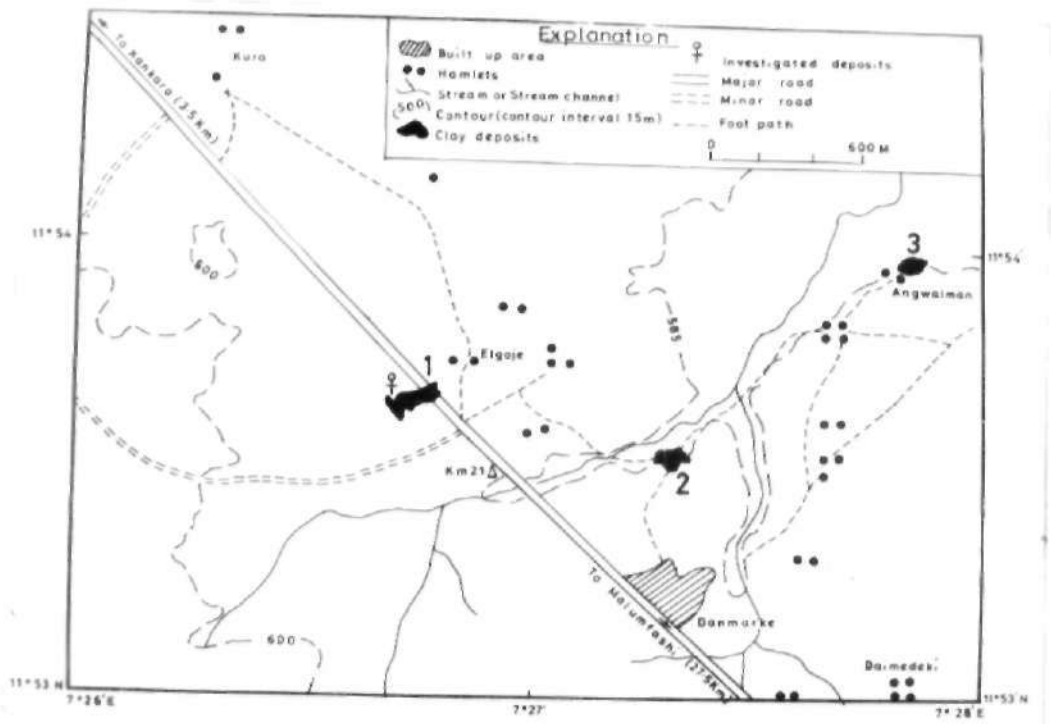
Most of the known kaolin deposits have been proven, by employing principally the time consuming and highly expensive reconnaisance borehole techniques. Borehole techniques, albeit the optimum geological method of prospecting are prone to several limitations. These include, the limited number of boreholes that can be made in a particular site, the limited quantity of borehole samples available for analysis, the inability to obtain representative bore samples as the bore is susceptible to disintegration in soft, loose and running ground, and also to obstruction by boulders (Kreiter; Kirsch; 1968)

From the foregoing it is evident that the data obtained from bore-holes can only provide limited information on the quality and quantity of these reserves. Consequently, where applicable borehole investigations should be supplemented by methods of applied geophysics. Considerable drilling effort, time and expense would be saved in the preliminary stages of an exploratory programme for kaolin deposits by the application of a combination of feasible, relatively rapid and cheap geophysical surveys to elucidate the best sites for test drilling.

1.2 THE KANKARA KAOLIN DEPOSITS

The Kankara kaolin deposits lie within an area bounded by latitudes 11°53' and 11° 55'N and longitudes 7°26' and 7°28'E, and extends over an area bordering Elgoje, Danmarke, Angwaliman and Yargoje villages (Map 2). The three deposits are completely buried under variable thicknesses of overburden and occur in sporadic lenses of varying sizes and geometry, (Oyeka, 1976).

Several exploratory trips to the sites have been undertaken by geologists. The first geological work on the first deposit (Kankara I) was carried out on behalf of an insecticide manufacturing company based in Jos. Several pits were sunk and some opencast paddocks around the old workings were opened. The resulting shafts were later examined by members of staff of the geological survey. Their work was followed by a more detailed investigations conducted by economic geologists of the same unit. From their investigation the proved reserves of lenses of pure and contaminated kaolin in Kankara I, and II are of the order of 1.15×10^6 and 2.28×10^6 metric tons respectively. A major setback in the above analysis was that the banka drilled boreholes seldom strike the bottom of the kaolin. This would imply that bodies of kaolin underlying a certain depth were excluded in the assessment.



Map 2: Location map of Kankara Kaolin deposits.
(Oyoka, 1976.)

Recent geological evidence also indicated the need for further work on the western edge of the Kankara I deposit (Map.4).

The present report commemorates the genesis of geophysical work on the prominent Kankara kaolin deposits. Detailed work on the Kankara I deposit, employing a combination of electrical resistivity, gravity and seimic methods was conducted by the author between October and December 1976. An area of 24 x 10^4 m^2 about an arbitrary reference point was surveyed (Map 4). The objectives of the survey were to supplement the existing literature on the deposit by (1) procuring reliable estimates of the reserves and associated geophysical parameters of the deposit and (2) to ascertain the best choice of geophysical methods in the exploration of kaolin deposit.

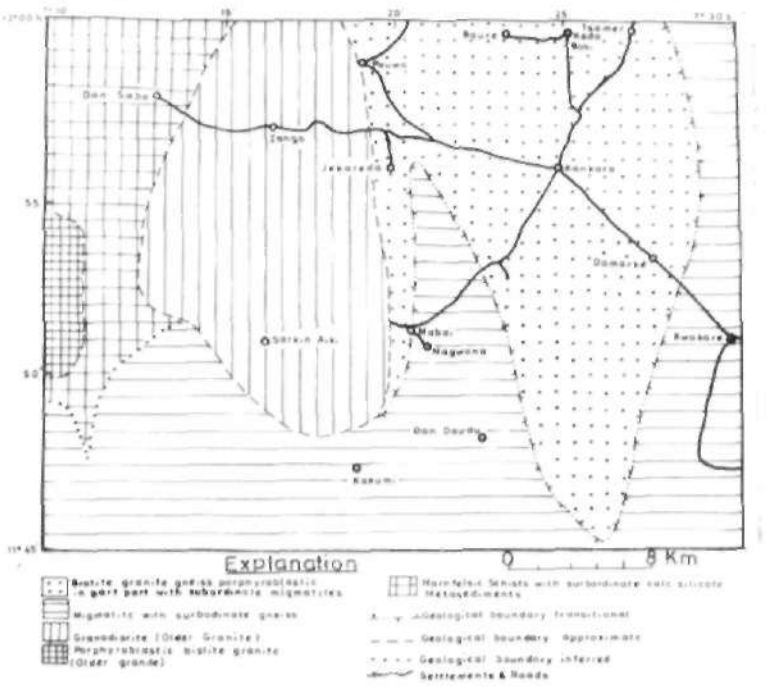
CHAPTER TWO

GEOLOGY

2.1 GENERAL GEOLOGY

The Kankara area is situated in the NNE section of the 1:100,000 standard sheet 78, Funtua (Map 3). The entire area of this section is underlain by rocks of the Basement complex, consisting mainly of migmatites, granite gneiss, biotite gneiss, metasediments of generally amphibolite facies metamorphism, and granitic rocks of the older granite suite (Ajibade, 1976).

The area considered in this report is underlain by mica shist, dipping generally SE at angles varying from 27^{o} to 43^{o}. The geological formation in the vicinity strikes generally EW and outcrops of the host mica-schist can be found along the river channels. The rock in situ occurs as silvery to light grey on the weathered surface and dark grey to dark greenish grey on the fresh surface, interspersed with injections of quartzo - feldspathic veins along fracture planes. It is generally fissile and readily parts along the cleavage planes. Beyond the mica-schist, the surrounding areas are occupied by biotite - granite - gneiss. A ridge of foliated weathered pegmatite with the foliation direction parallel to the local strike is found in the southern part of the surveyed area. The rock has low SE angle of dip varying between 22^{o} and 40^{o}, (Oyeka, 1976)


Explanation
0
8 Km
Biotite granite gneiss porphyroblastic
Migmatite with subordinate gneiss
Granodiorite (Older Granite)
Porphyroblastic biotite granite
(Older granite)
Metasediments
Geological boundary Approximate
Geological boundary inferred
Settlements & Roads

2.2 GEOLOGY OF THE KAOLIN DEPOSIT

The Kankara I deposit is situated 4.5 km SE of Kankara town near the Elgoje village in the Malumfashi - Kankara - Katsina Road (Map 2).

The deposit lies in a moderately wooded forest reserve bordered on the SE side by a stream channel running approximately EW. The area is lightly cultivated and is characterized by a relatively flat terrain. The prevailing low relief is controlled by metasediments and the absence of major intrusions, (Oyeka, 1976).

No natural exposures of the deposits occur in the vicinity but local mining under the overburden which has been in existence as far back as half a century ago has exposed the mineral in pits P_1 and P_3 (Map 4). In vertical section (Figure I.I) the general sequence from surface to bedrock is as follows:

(1) an overburden of variable thickness ranging from 1 m to 25 m, but averaging 5 m. The overburden consists generally of dark brown earthy clay - overlain by a thin layer of loose brown top soil, and underlain by a layer of mottled, weathered earthy clay.

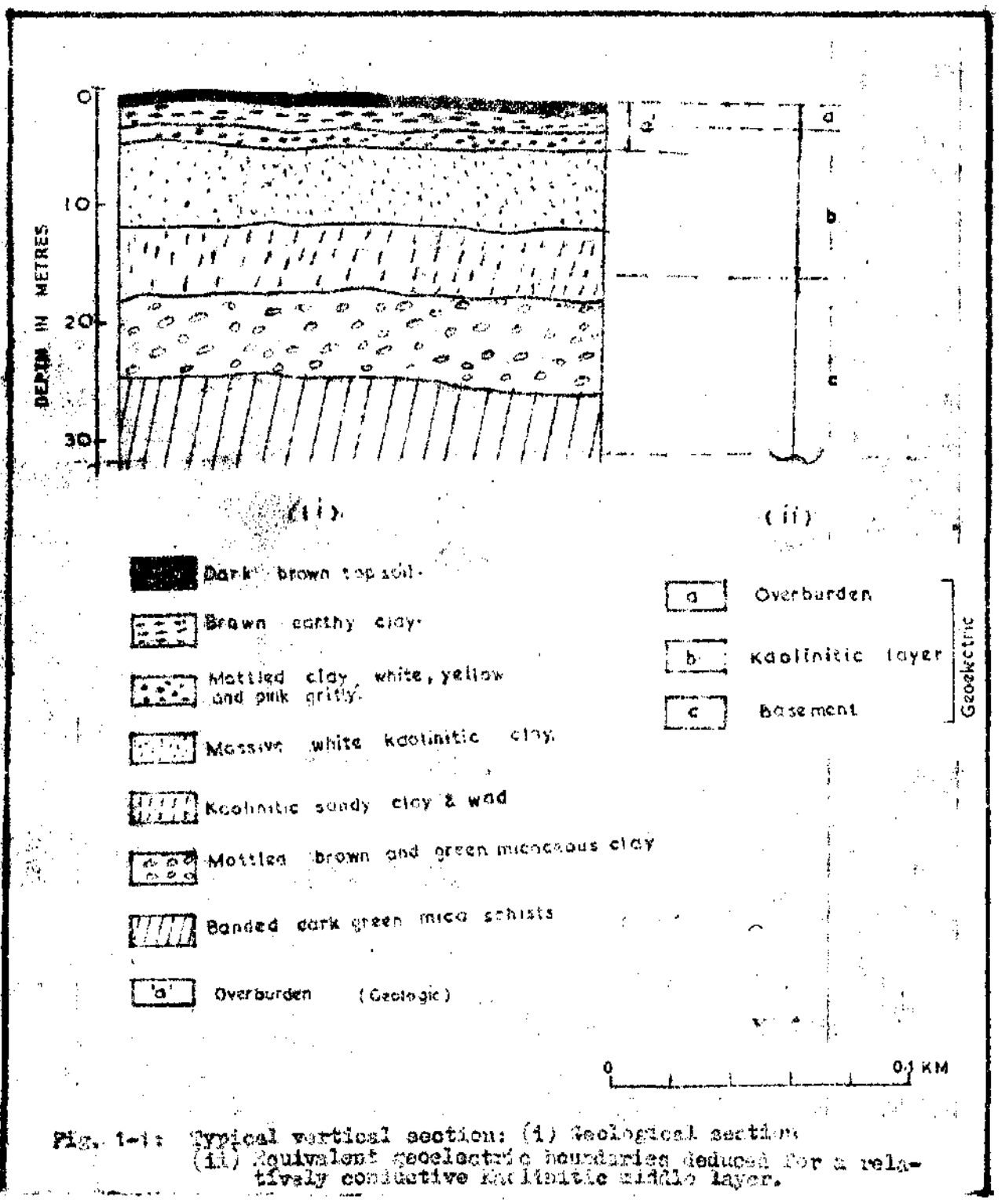


Fig. 1-1: Typical vertical section: (i) Geological section (ii) Equivalent geoelectric boundaries deduced for a relatively conductive kaolinitic middle layer.

(2) a massive section of white kaolinitic clay overlying a region of variegated clay bearing ramnant quartz and muscovite.

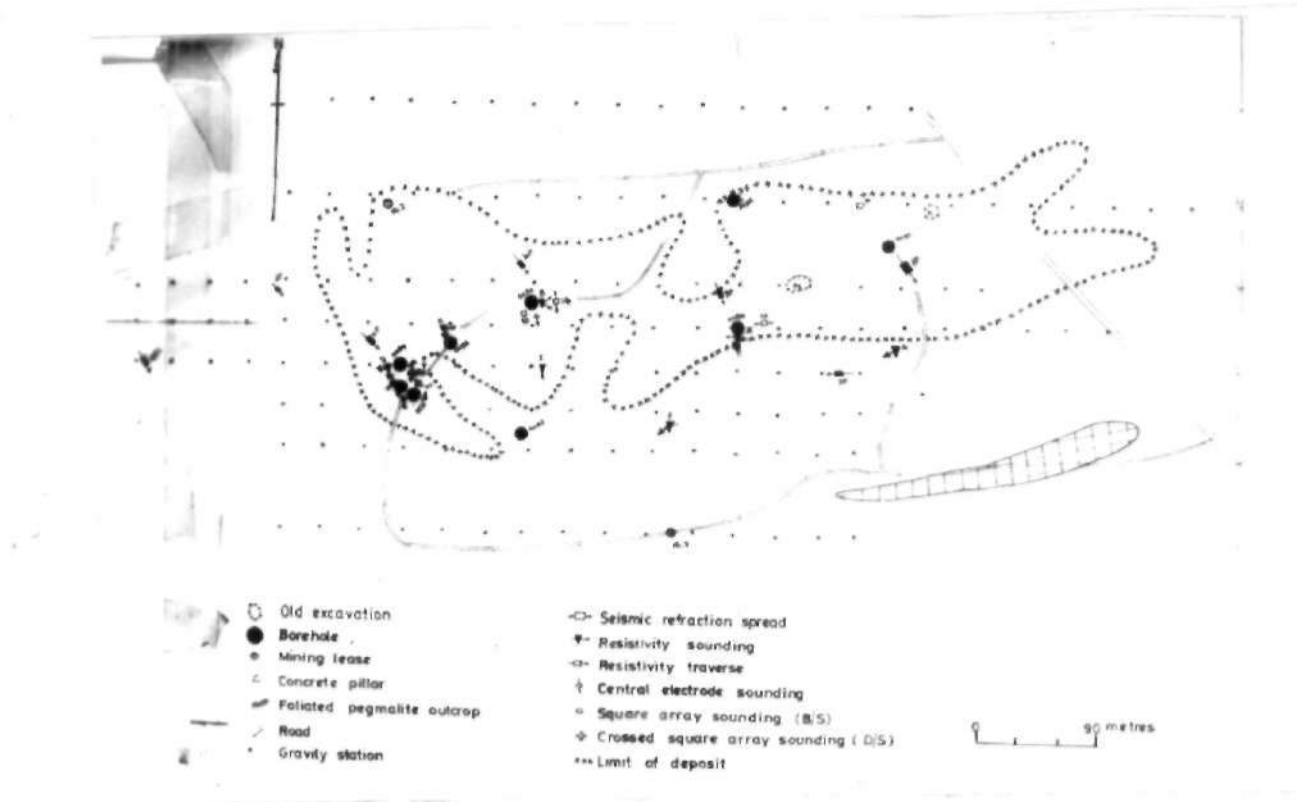
(3) Banded dark green mica-schists.

An outcrop of hard, compact, mottled and heavily Leached pitchstone is exposed in pit P1. In place the rock is a weathered, vesicular, sill-like body pinching off to the west.

Structurally the deposit exhibits no evidence of slikensides or slumping (Oyeka, 1976),

The Kankara kaolin is a primary deposit, the main source of which is the emplaced slightly manganiferous, feldspar - rich pegmatite. The clay occurs sporadically in lenses of kaolinitic bodies intergraded with or surrounded by pink to brown micaceous.clay with no definite geometrical pattern. Quartz grains, small amounts of zircon, sphene, ilmenite and tourmaline unaffected by oxogenic processes are present in the kaolin as minor impurities (Oyeka 1976) Characteristically the kaolinitic clay is stiffly plastic, generally creamy white in colour but with areas of yellow and brown mottling. Results of recent drilling and sub-sequent logging of boreholes indicate that the mineral is of two main varieties; (1) an outer contaminated portion

often gritty, ferruginized in places, bearing mainly remnants of decomposed off-white feldspar; and (2) an inner, relatively purer, less gritty white clay. Black manganese oxide occuring as wad and regularly associating with green, chloropal is encountered in localized concentrations.



Map 4: Geophysical survey map.

CHAPTER THREE

PRELIMINARY ANALYSIS AND FIELD TECHNIQUES

3.1 PRELIMINARY ANALYSIS

When sufficient geological evidence is available to substantiate the geophysical result it is often expedient to procure a pre-knowledge of what is likely to be the field response before taking measurements on the field. The appropriate techniques to be used, the cost and the duration of the survey all owe a great deal to such analyses. In this chapter an account of the pre-field analyses made on the resistivity, gravity and seismic methods is given. The analyses were carried out a month prior to the actual field work and were based on the available borehole information, published geophysical parameters, and Laboratory measurements. The resulting models from such analyses could be interpreted tentatively as the ghost reflections of the anticipated field results.

3.1 RESISTIVITY

From table 3.1 a significant resistivity contrast exists between the kaolin mineral and the surronding formations, thus justifing the execution of the pre-resistivity work. The records of the boreholes however show superflous

subdivision of layers which although differ invariably in lithological compositions, lack resistivity contrast, Such layers therefore constitute a single geoelectric layer. On the average, 3 geoelectric layers are apparent in the area of study. For convenience these layers are designated overburden, kaolinitic layer and bedrock.(Fig. 1.1).

Pre-determined borehole geoelectric layer thicknesses with the appropriate standard resistivity values from table 3.1 were computer processed using a programme (Verhenjen 1975) designed to yield theoretical Schlumberger sounding curves.

The results obtained from several boreholes indicated that the deposit is characterized by the simple H-type Schlumberger sounding curves (Fig. 3.1). From Fig. 3.1 (a) it is apparent that in areas where drilling information is lacking the exact subsurface structure would be obscured by the effect of layer suppression and equivalence. The suitability of a resistivity survey in such areas is therefore uncertain as this would lead to severe pseudoanisotropy (Zohdy and Eaton 1974).

The equivalent geologic sections for the 3 - layer Schlumberger - curves are also illustrated in Fig 3.1. These models were obtained by imposing plausible imaginary

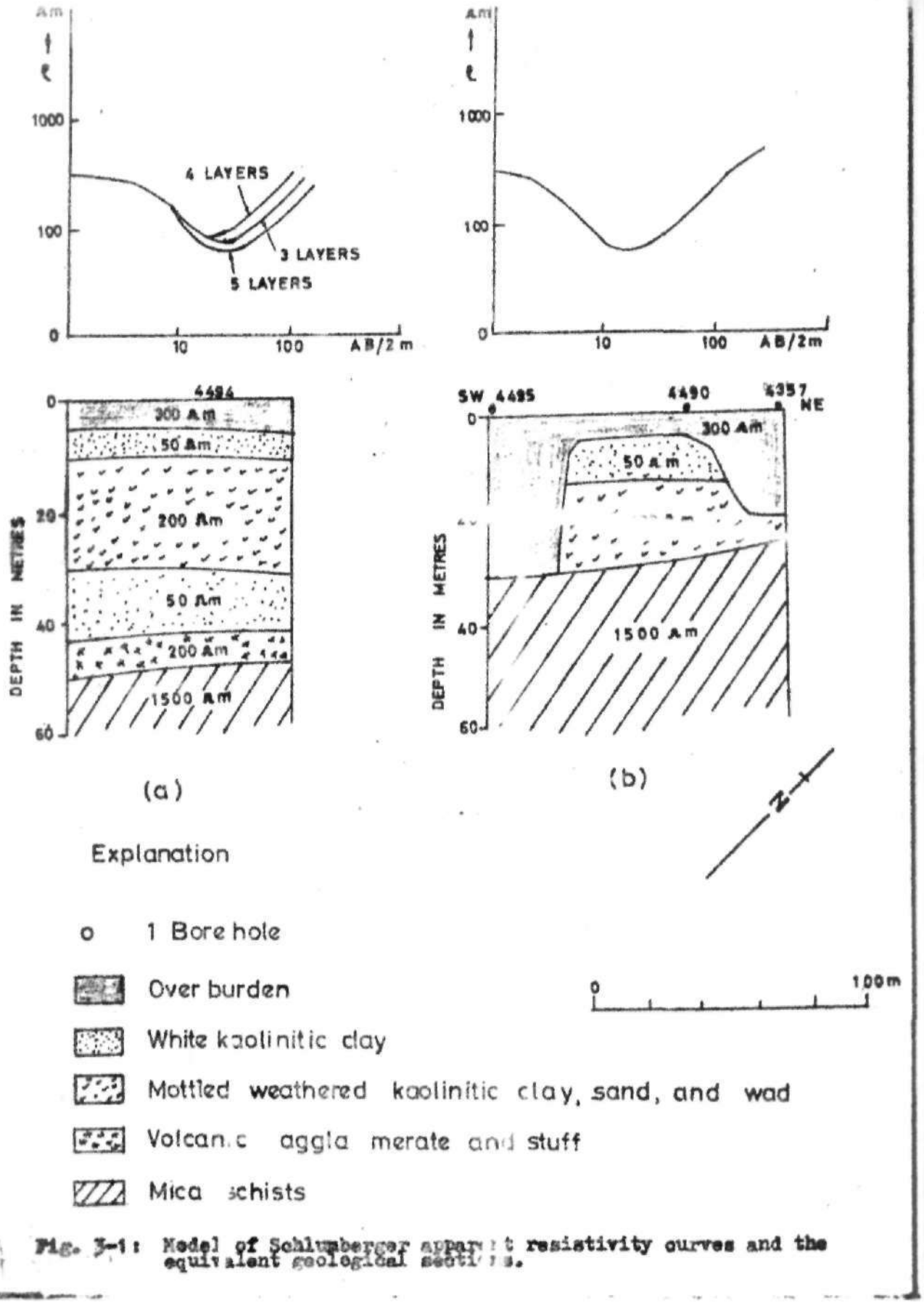


Fig. 3-1: Model of Schlumberger apparent resistivity curves and the equivalent geological sections.

geologic boundaries between neighbouring boreholes. The model Fig. 3.1 (b) exhibits the sporadic occurence of the deposit. The model also reveals the possible existence of vertical or inclined contacts.

3.1.2 Gravity

Densities of rock samples collected from different locations in the anomalous zone were determined using the procedure outlined by Parasins (1954), whereby dry and saturated densities are evaluated. The results obtained are contained in table 3.2 (a).

Using the mean densities of 1.61×10^3 kg/m^3 and 2.76×10^3 kg/m^3 for the kaolin and mica-schists respectively, in the equation:

$$\Delta g = 2\pi G \Delta\sigma h$$

Where Δg would be anomaly maximum, G is the universal gravitational constant, $\Delta\sigma$ is the density contrast, and h is the average thickness of the zone of anomalous density; it is evident that a gravity survey would yield negative Bouguer anomalies which would vary with the thickness. Table 3.2 (b) below shows the magnitude of the anticipated gravity anomalies.

3.1.3 Seismic

A high velocity contrast (quote fig. I) between the kaolin mineral and the bedrock is anticipated from table 3.1. A seismic Survey would thus in general be capable of mapping the bedrock and under favourable condition may yield measures of depth to mineralized zones. The suitability of this technique in the present task, may however be limited by the sporadic behaviour of the deposit, the possible effects of velocity inversions and the blind zones episode.

3.1.4 Magnetic

Laboratory measurements of magnetic susceptibilities, yielded values of 6 to 8 x 10^{-5} and 4 to 7 x 10^{-5} S.1 units for the kaolin and the bedrock respectively. A magnetic survey would thus not be appropriate in view of the inadequate magnetic susceptibility contrast. This confirmed a similar observation by Nkuesenam (1976).

3.1.5 Conclusion

On the basis of the foregoing analyses and the available geological information the resistivity and gravity methods would be well suited to the problem. Seismic refraction survey may also yield important information under favourable conditions. Magnetic methods would not be appropriate to the task at hand.

TABLE 3.1

Physical Parameters of typical Rock materials in the survey area

Rock type	Resistivity Range (Ω m)	Seismic Velocity (m/s)	
		Dry Rock	Wet Rock
Clayey Earth' soil	10^2 - 4 x 10^2	110 - 305	1380 - 1680
Sand (buried)	1.2 x 10^2 - 1.1 x 10^3	600 - 1850	
Kaolin	1 - 1.2 x 10^2	915 - 1520	1380 - 1680
Mica schists	10^3 - 10^5	6400 - 7000	
Gneiss	10^2 - 10^5	3540 - 7500	1370 - 3050
Marble	10^2 - 10^8	3750 - 6900	
Volcanic tuff		216	
Weathered layer		300 - 900	

TABLE 3.2

(a) Results of density measurements

Rock types	No of samples	Range of Dry density x 10^3 kg/m^3	Mean Dry density density x 10^3 kg/m	Range of saturated density x 10^3 kg/m	Mean saturated density x 10^3 kg/m	Overal mean density x 10^3 kg/m
Clay	6	1.69 - 2.48	2.18 ± 0.26	1.78 - 2.52	2.26 ± 0.26	2.22 - 0.26
Kaolin	5	1.58 - 1.63	1.61 ± 0.02			
Sandstone	2	2.33 - 2.34	2.34 ± 0.01	2.36 - 2.39	2.38 ± 0.01	2.36 ± 0.20
Pegmatite	8	2.47 - 2.64	2.52 ± 0.10	2.52 - 2.64	2.58 ± 0.04	2.55 ± 0.06
Mica Schist	2	2.74 - 2.77	2.76 ± 0.03			

(b) Anticipated anomaly (g.u.) for various borehole thicknesses.

Borehole	Thickness	Density contrast kg/m^3	Anomaly (g.u)
4494	14	- 1.15	- 6.75
4490	4	"	- 1.93
4495	3.2	"	- 1.60
4499	2	"	- 0.96
4489	14.5	"	- 6.99
4373	20	"	- 9.64
4492	1.2	"	- 0.58
4493	4	"	- 0.48
4497	3	"	- 1.45

3.2.1 FIELD TECHNIQUES

The field party consisted of the author, one field assistant provided by the Department of Physics and three local unskilled labourers. The field operations were designed to achieve entire coverage of the anomalous zone in the limited time available. 21 days were spent on the field.

A grid pattern was adopted in the construction of the field network in view of the predominant gentle topographic relief and the sporadic occurence of the deposit. The approximately central BH, 4494 borehole was taken as the reference position (Map 4). 150 m, N and S, 500 m, W and 300 m, E of this reference mark was surveyed. A zero traverse (base line) running EW was defined through this reference. 8 EW traverses each about 400 m long were established at 30 m. intervals from one another, lying N and S of the zero traverse (Map 4). Stations were staked at 30 m intervals, along each traverse. For easy location of points on the grid cross-section traverses are designated according to their distances and directions from the zero traverse, for example, the zero traverse together with the first two adjacent N and S traverses are labelled in ascending order as 60 S, 30 S, 00, 30 N and 60 N. The

4th station along traverse 30 N and W of the zero traverse is designated 30 N/4 W. Traverses were extended well beyond the anomalous zone inorder to adequately define the flanks of the anomalous zone.

Measurement paths were cleared inorder to avoid damage to cables and also to provide good visibility. A sketch plan of the area of study including the positions of the sites at which resistivity depth probes and profiling traverses, gravity and seismic refraction measurements were made is shown in Map 4.

The geophysical instruments used were provided by the Department of Physics and consisted of a theodolite; a Megger Earth Tester, Worden gravimeter No. 135 and an FS-3 facsimile seismograph. Detailed description of these equipment are given under the relevant section of the thesis.

The instruments were conveyed daily to the site in the departmental van. They were thoroughly checked and calibrated where applicable at home before the routine field work. On the field, occasional checks were made by method of repeated readings.

The ground elevations of the various stations were established by a level survey employing a theodolite. The

resulting surface levels were finally reduced to the datum height 21.2 m at the reference BH 4494. A closure error of 0.02 m was obtained which is acceptable for all purposes.

The number of observations made were as follows:

(a) Resistivity:
- 7 Schlumberger array, Electric sounding stations.
- 2 Central electrode sounding.
- 2. Square array soundings.
- 1 Cross square array sounding.
- 7 Wenner array, Electric Profiles.

(b) Gravity: A total of 150 levelled detailed stations at an average spacing of 3 m were occupied.

(c) Seismic Refraction: A total of 8 records were obtained from 4 spread (30 m - 40 m) on three traverses.

CHAPTER FOUR

RESISTIVITY SURVEY

4.1 INTRODUCTION

The method permits direct detection of the mineralized zone due to resistivity contrast between the mineral and the formations in juxtaposition. The physical parameters measured in the field determination of resistivity are the earth resistance between two measuring points of known separation and the current electrode separations. The resistivity method like the gravity and magnetic methods of geophysical prospecting is based on potential theory and therefore lacks a unique solution. Correct interpretation can only be offered by correlation of several sounding curves with the available geological information, and also by traversing the area with horizontal resistivity profiles.

In this chapter a report on the resistivity survey employing a combination of different electrical sounding methods, and constant traverses (profiling) is given. The basic arrays utilized are shown in Figs. 4.1 and 4.2.

4.2 INSTRUMENTATION

The resistivity equipment consisted of the portable Evershed and Vignoles Megger Earth Tester. This instruments is self contained, incorporating a hand driven generator and an ohmmeter in a strong hard wooden case. In the field operations, a periodically reversed direct current produced from the hand generator was introduced to the ground via two copper current electrodes C_1 and C_2, which were driven a known distance into the ground at a pre-determined separation; the resulting periodically reversed potential difference between two similarly placed potential electrodes P_1 and P_2 was then applied to the input terminals of the instruments. The ensuring current was rectified and passed through the deflecting coil of the ohmmeter, so that the resistance in ohms was read directly on a logarithmic scale as the ratio of the voltage at the input terminals to the current through the output terminals of the instrument - the familiar cross - coil ohmmeter principle.

At each measurement point the instrument was calibrated as prescribed by the manufacturer. This involved manipulating the rheostat knob in the adjust position until the pointer was stationary over the red datum mark on the scale.

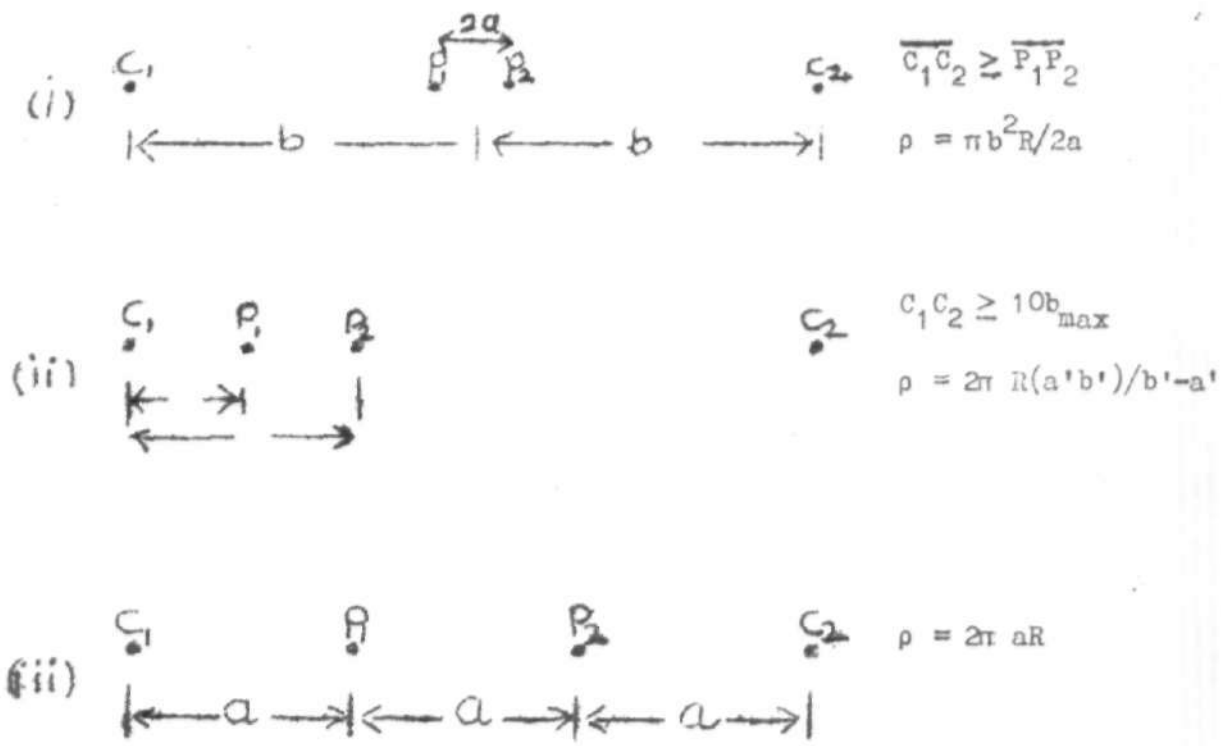


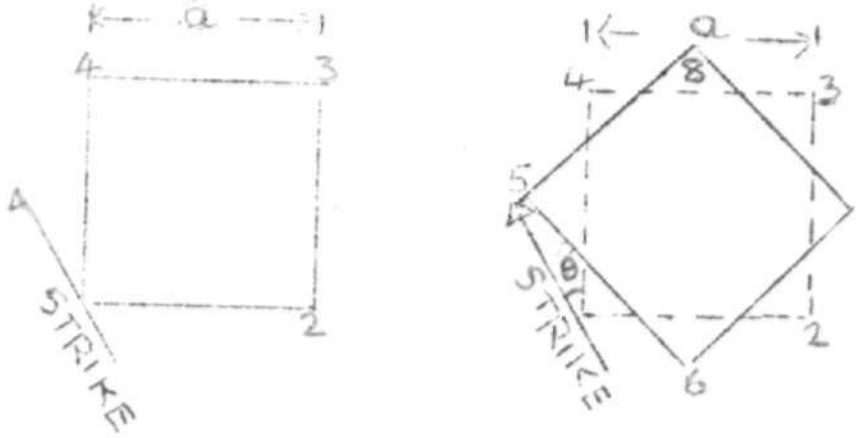
FIG 4.1 The electrode arrays used and the corresponding formulas for apparent resistivity.

(i) Schlumberger Sounding carry,

(ii) Central electrode Sounding array and

(iii) Wenner profiling array.

C_1 and C_2 are current electrodes, P_1 and P_2 are potential electrodes. R is the observed resistance and ρ is the corresponding apparent resistivity for the Configuration.



Configuration	electrode positions 1 2 3 4 5 6 7 8	observed resistance
α	C P P' C'	$R_\alpha = R_1$
β	C C' P' P	$R_\beta = R_3$
γ	C P C' P'	R_γ
α'	C P P' C'	$R'_\alpha = R_2$
β'	C C' P' P	$R'_\beta = R_4$
γ'	C P C' P'	R'_γ

Fig. 4.2 Layouts of simple and crossed square arrays.

Contact resistance was reduced to a minimum by the application of salt water to the ground in the vicinity of the electrodes. The observed resistances have a measurement error of about 10%. The other associated errors in the resistance values are those caused by the effects of heterogeneity, anisotropy, layer suppression and equivalence.

4.3. RESISTIVITY SOUNDING

Resistivity sounding furnishes detailed information on the vertical succession of the various conducting zones and their individual thicknesses and apparent resistivities. In practice, however, the electrical sounding data are influenced by both vertical and horizontal heterogeneities. Therefore, for purposes of correct interpretation, crossed soundings as well as sounding with different arrays were utilized.

4.3.1 SCHLUMBERGER ELECTRIC SOUNDING

Using the Megger Earth Tester a succession of apparent resistivity measurements were made with an expanding current electrode separation, as the centre of the schlumberger electrode configuration and its orientation remained fixed for some selected values. The values chosen for the current

electrode separations were based on the geological evidence and for the present purpose current separations varying from 2 to 360 m were used for an anticipated maximum depth of 60 m. The potential electrode separations ranged from 1 m to 20 m depending on the magnitude of the measured voltage. The Schlumberger depth probes were executed in 7 main locations, and consisted of 4 NS, 3 EW, 3 NE - SW and 1 NW - SE measurements (Map 4). The choice of the sounding directions was however influenced by the wooded forest.

The apparent resistivities ρ_s were calculated from the field data using the expression.

$$\rho_s = \pi b^2 R/2a \quad \text{(Schlumberger array)}$$

Where a, and b represent half potential and half current spacing respectively and R is the observed resistance. The resulting apparent resistivities were plotted as a function of effective spacing employing as usual logarithmic coordinates.

The sounding curves obtained were of the H types and generally characterised by a sharp rise in the apparent resistivity values for higher electrode separations. The results conform fairly well with the model curves obtained

in the preliminary analyses (chapter three).

Qualitative Interpretations

The apparent resistivities of some selected profiles were plotted as a function of spacing on vertical lines located directly underneath the respective sounding points, using a linear scale, to suppress the effects of near surface layers. The apparent resistivity values were finally contoured to yield apparent resistivity sections. To examine the variation of apparent resistivity measurements with orientation, sections have been drawn for both NS and NE - SW traverses (Fig. 4.3, a and b). From the results it is apparent that the bulk of the mineral is concentrated in the horizon 3 - 12 m. The characteristic low resistivity of this zone is strongly manifested in th NE orientation. The dotted curves represent the profile of the abscissa values of the minimum points as observed on the various H-types schlumberger curves.

Quantitative Interpretation

The smoothed sounding curves were subsequently superimposed on the appropriate master curves (Rijkswaterstaat 1969), from which the various formation thicknesses and

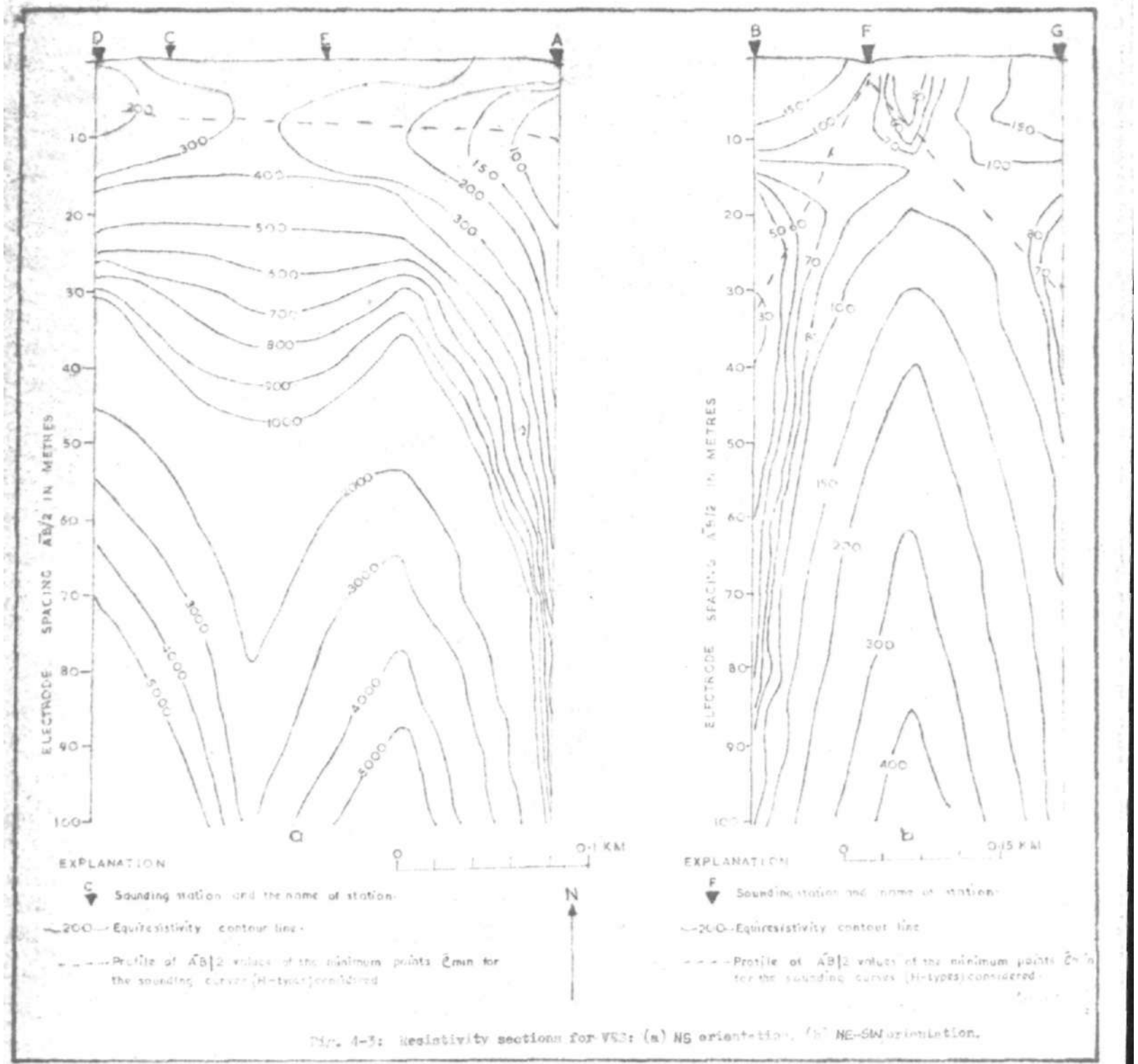


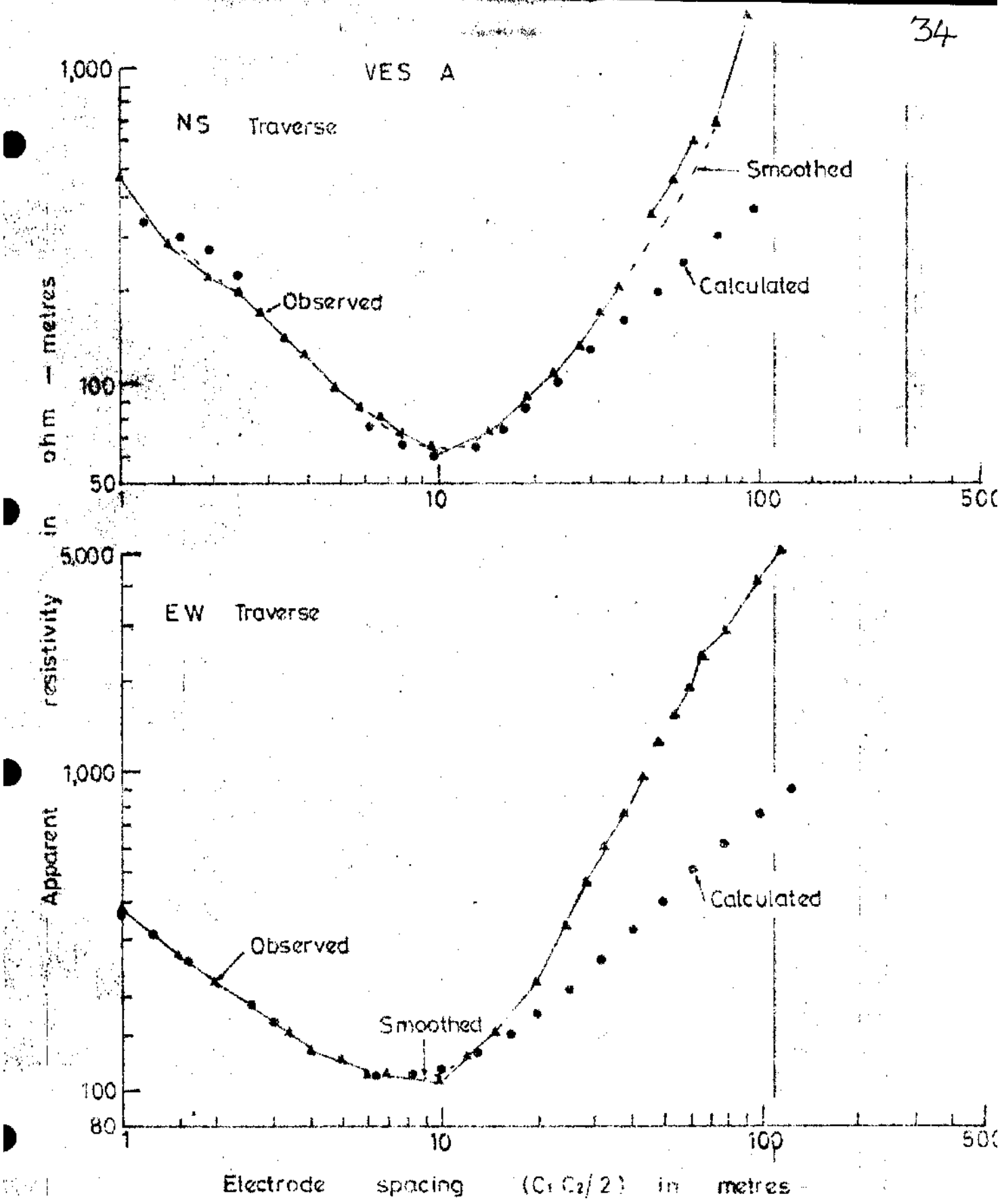
Fig. 4-3: Resistivity sections for VES: (a) NS orientation, (b) NE-SW orientation.

resistivities were deduced. Two - layer master curves of Bhattacharya and Patra (1968) were employed on occasions when matching with the 3 - layer master curves proved inadequate. The parameters obtained from the matching exercise were subsequently processed in the HP 9830 computer, obtaining final best fit theoretical curves after further rational adjustments.

Sounding at Location A

The vertical electrical soundings (VES) at this location were executed along two traverses, one to the NS and the other to the EW. The resulting sounding curves for the apparent resistivities measured are shown in fig. 4.4.

The sequence of resistivities on both curves indicates a 3 - layer set up - a near surface layer of resistivity over 350 ohm-m with an average thickness of about 1.2 m underlain by an anisotropic and conductive zone of about 11.5 m thick, followed by a highly resistive layer, corresponding presumably to the basement. The schlumberger curves attain a slope greater than one at the large electrode separations making the achievement of


VES A
NS Traverse
EW Traverse
Observed
Smoothed
Calculated
Apparent resistivity in ohm - metres
Electrode spacing (C1 C2/2) in metres
1,000
100
50
5,000
1,000
100
80
1
10
100
500

excellent fits between observed and calculated resistivity values impossible at depth. The results of the neighbouring borehole log 4494 drilled to a depth of 54 m reveals a 6 - layer structure in which the third layer, consisting of volcanic agglomerate, sand and wad is sandwiched between two low resistivity covers of predominantly kaolinitic clay. Correlation of the sounding results with the above set-up shows consistently that the electrical basement is at a higher elevation than the basement complex in the vicinity. The result is reflective of either (1) the possible existence of a vertical fault over the highly resistant rock formations with the centre of the configuration over the down thrown compartment.- the absence of sharp peaks in the EW orientation is consistent with the results obtained for electrical soundings perpendicular to fault planes (Kunetz, 1966); or (2) the situation where the current electrodes go beyond the kaolin deposit.

The horizon 31 - 42 m according to the available borehole information bears the lower bulk of kaolin mineral. With a detectability of less than 35% this layer is obviously suppressed in the Schlumberger curves. The geoelectric horizon (1.2-12.7 m) of kaolinitic clay manifests its presence largely by its horizontal

conductivity, with the result that layers which present the same ratio of thickness to apparent resistivity will be electrically equivalent. Koefoed has demonstrated through mathematical analysis based upon the properties of the raised kernel function, a graphical method of determination of equivalent cases (Fig. 4.10). The value of Koefoed coeficient of the first order term "c" has been deduced for each VES using the appropriate combination of d_2, ρ_2 and ρ_3 values obtained from the modelling exercise (table 4.1 (a). The parameters of the equivalent cases are determined by multiplying the abscissa and ordinate values of the predetermined point on the curve of equivalence by C and ρ_3 respectively. The combined coefficient of anisotropy for the VES A geoelectric section was found to be 0.85.

Sounding at location B

The resistivity depth probe measurements at this location were made along NE-SW and NW-SE traverses. Fig 4.5 (a) shows the VES curves obtained from both the NE-SW and NW-SE orientations. The forms of the curves manifest the presence of strong lateral heterogeneity in the subsurface structure which may be attributed to the

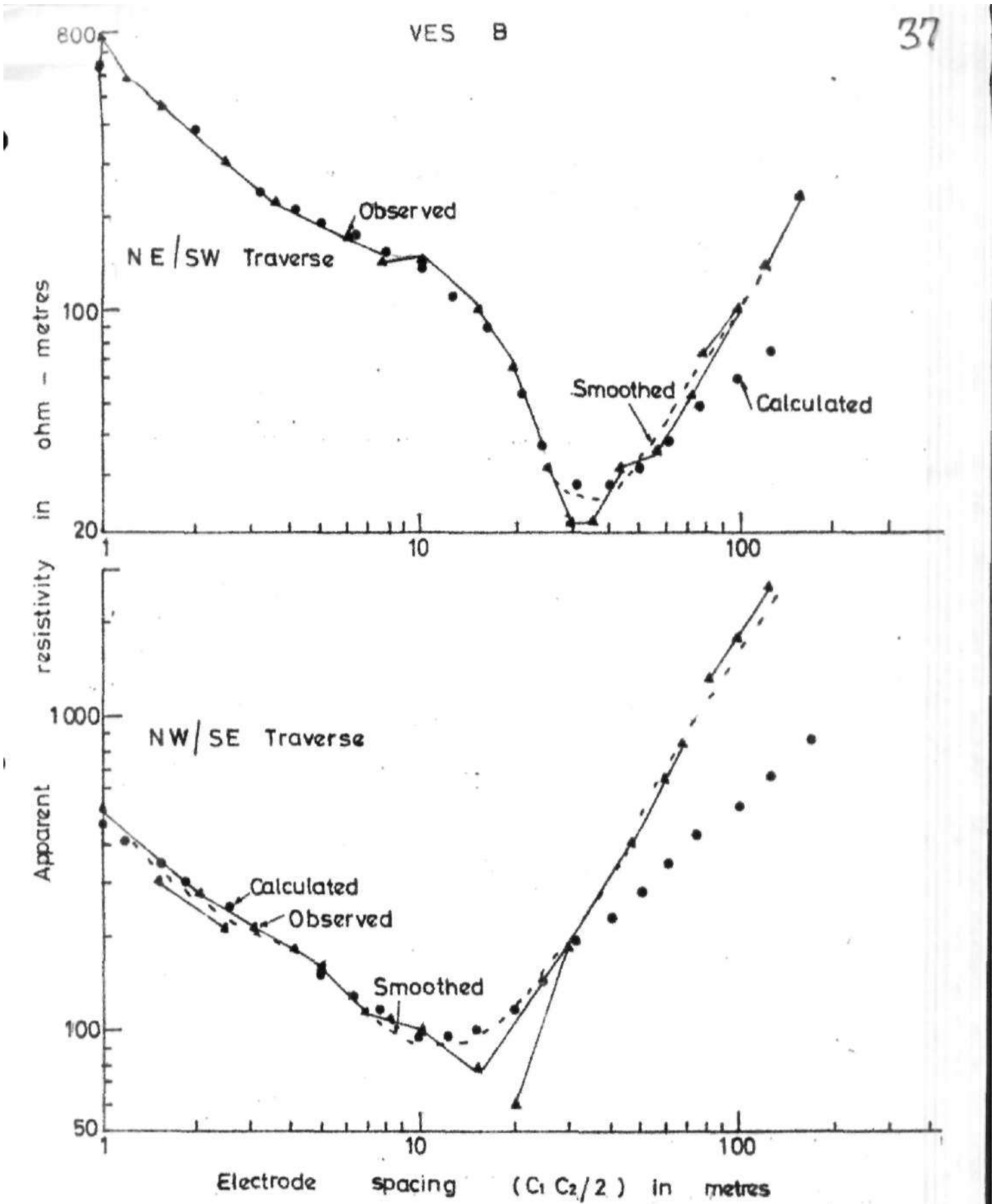


Fig. 4-5: (a) Interpretation of VES B curves in terms of a 4-layer model

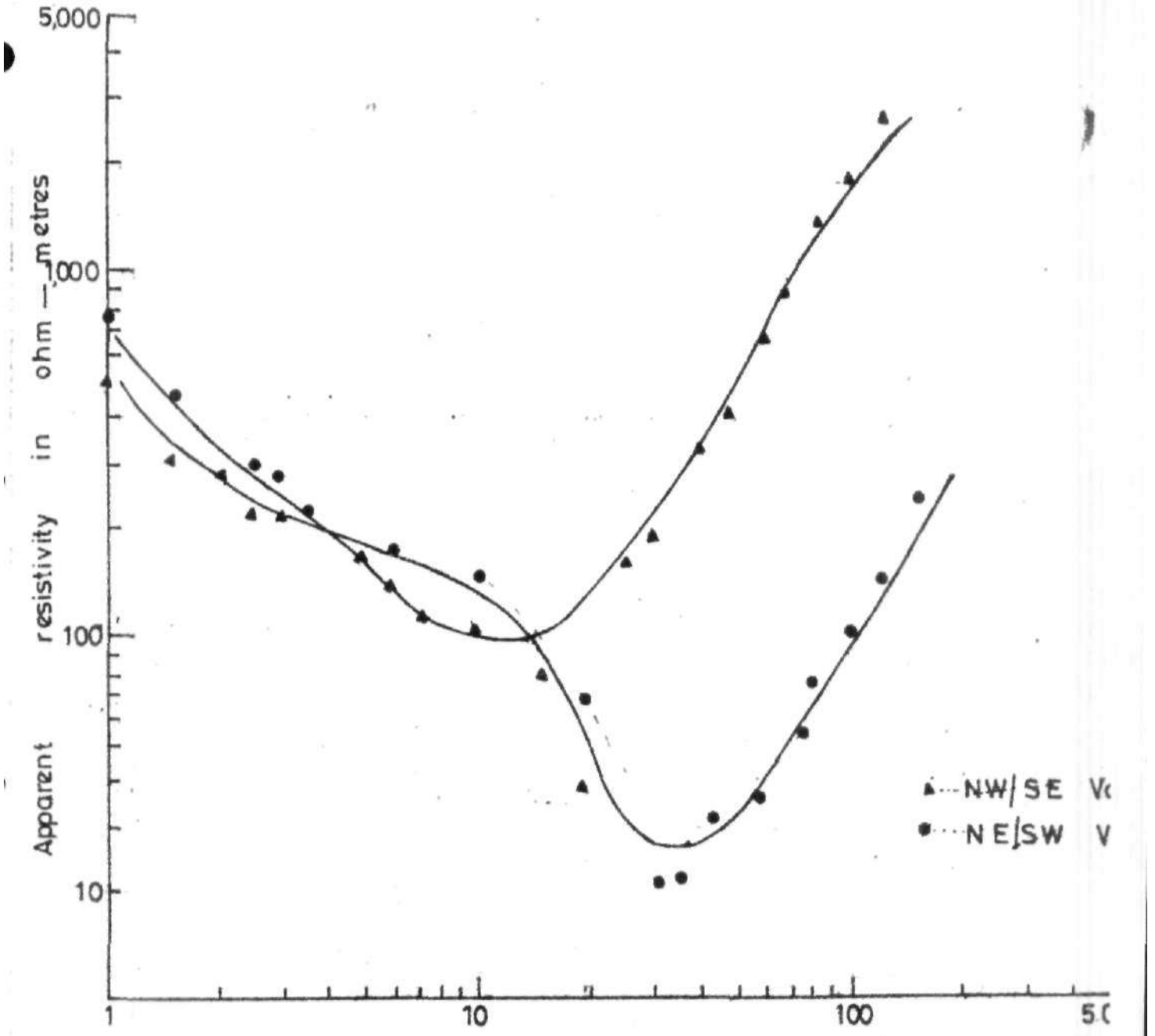


Fig. 4-5 (b) Comparison of the VES B curves.

presence of probable contacts. The curves are interpreted in terms of a 3 - layer geoelectric section (table 4.1 (a)), after the removal of the cusps caused by the current electrode crossing conductive lateral inhomogeneities by visual smoothing. Interpretation in terms of a 4-layer (table 4.1 (b))geoelectric section using two layer master curves and the auxiliary point charts (Bhattacharya and Patra 1968) has also been considered. The scatters observed at shallow spacings in the NW-SE traverse reveals that the plane of contact is presumably in the NE-SW direction, and represents the case of the initial crossing of the contact by a current electrode. Comparison of the two curves in fig 4.5 (b) shows that they both intersect one another at the 13 m electrode spacing which probably establishes the maximum depth of contact. The scatter of the field data (approximating a trough) within this region suggest that the first two beds in contact probably terminate in a more resistant bed. The similarity of the curves beyond this point both uplifting the highly resistant basement suggests that the contacts have been crossed and measurements are now within a contact free region.

The borehole data reveal the presence of an overburden down to a depth of 3.45 m and a basement elevation of 26 m. The discrepancy between the geoelectic and borehole thicknesses can be attributed in part to the electrical anisotropy of the beds.

Sounding at location C

The apparent resistivities obtained along the NS and EW traverses at this location are shown plotted graphically (fig 4.6) as a function of effective spacing. Two interpretations are possible after careful examination of the curves.

A 3-layer case is apparent from the data after the smoothing exercise (table 4.1(a)). The observed large scattering in the data may be attributed to the rapidly changing soil properties with increasing depth.

A thorough examination of the EW VES curve reveals an angular peak followed by an angular trough, approximating a dike of thickness 10 m, encamped in low resistivity formations. The prevailing low resistivity contast is demonstrated by the blunt - shaped peak and trough. The sharp increase in resistivity values beyond the dike is indicative of the presence of an insulating sub-stratum.

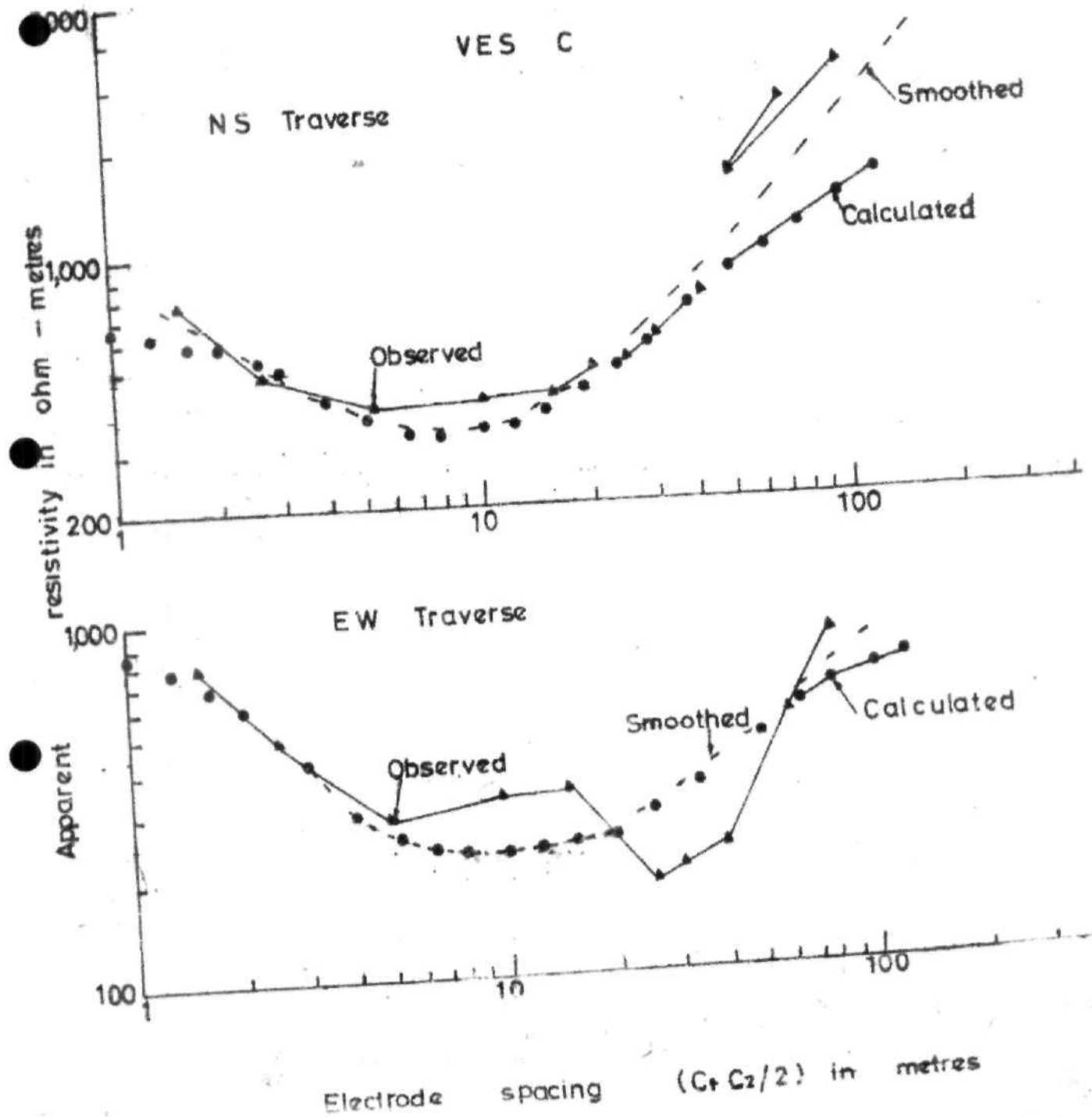


Fig. 4-6: Interpretation of VES C curves in terms of a 3-layer model.

Sounding at Location D

The sounding curves computed from the resistivity measurements made along traverses to the NS and EW are shown in fig 4.7. Both curves reveal a 3-layer section. The sharp rise in the apparent resistivities obtained for the NS traverse is compatible with the presence of vertical contact underlain by an insulating sub-stratum. The validity of the above interpretation is borne by the logs of the neighbouring boreholes 4499 and 4489 which are about 14 m apart. The log of 4499 shows an overburden of thickness 26 m underlain by a kaolinitic layer of thickness 2 m, while an overburden of thickness 2 m underlain by a kaolinitic layer of 7 m is depicted in log 4489. After careful examination of the borehole data (Map 5) the sharp rise in resistivity values for EW traverse could be attributed to the fact that for increasing electrode spacing the current electrodes expanded beyond the kaolin deposit into a more resistant subtratum.

Sounding at Location E, F and G

The apparent resistivity values derived from these soundings are shown graphically in figs 4.8 and 4.9.

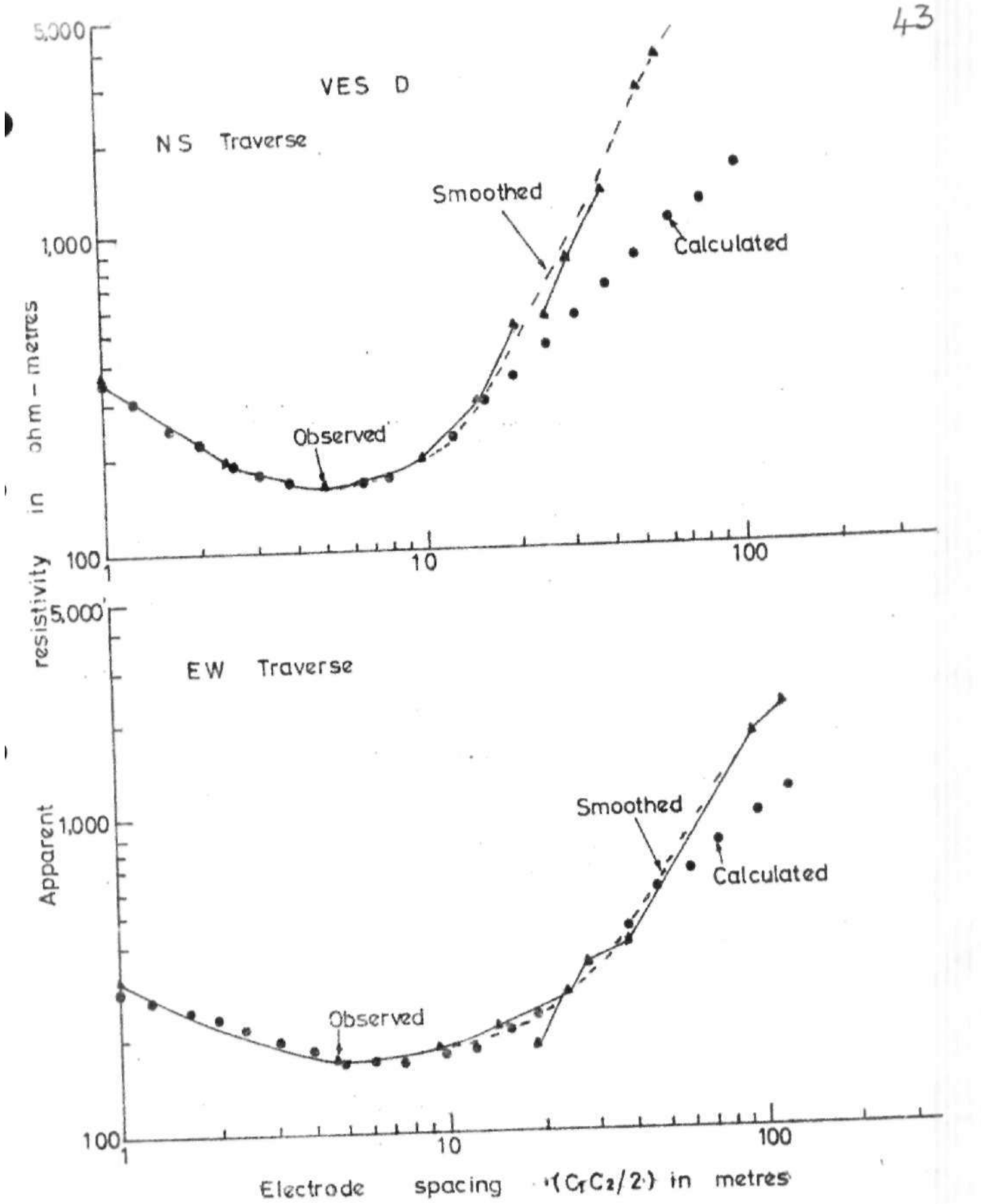


Fig. 4-7: Interpretation of BES D curves in terms of a 3-layer model.

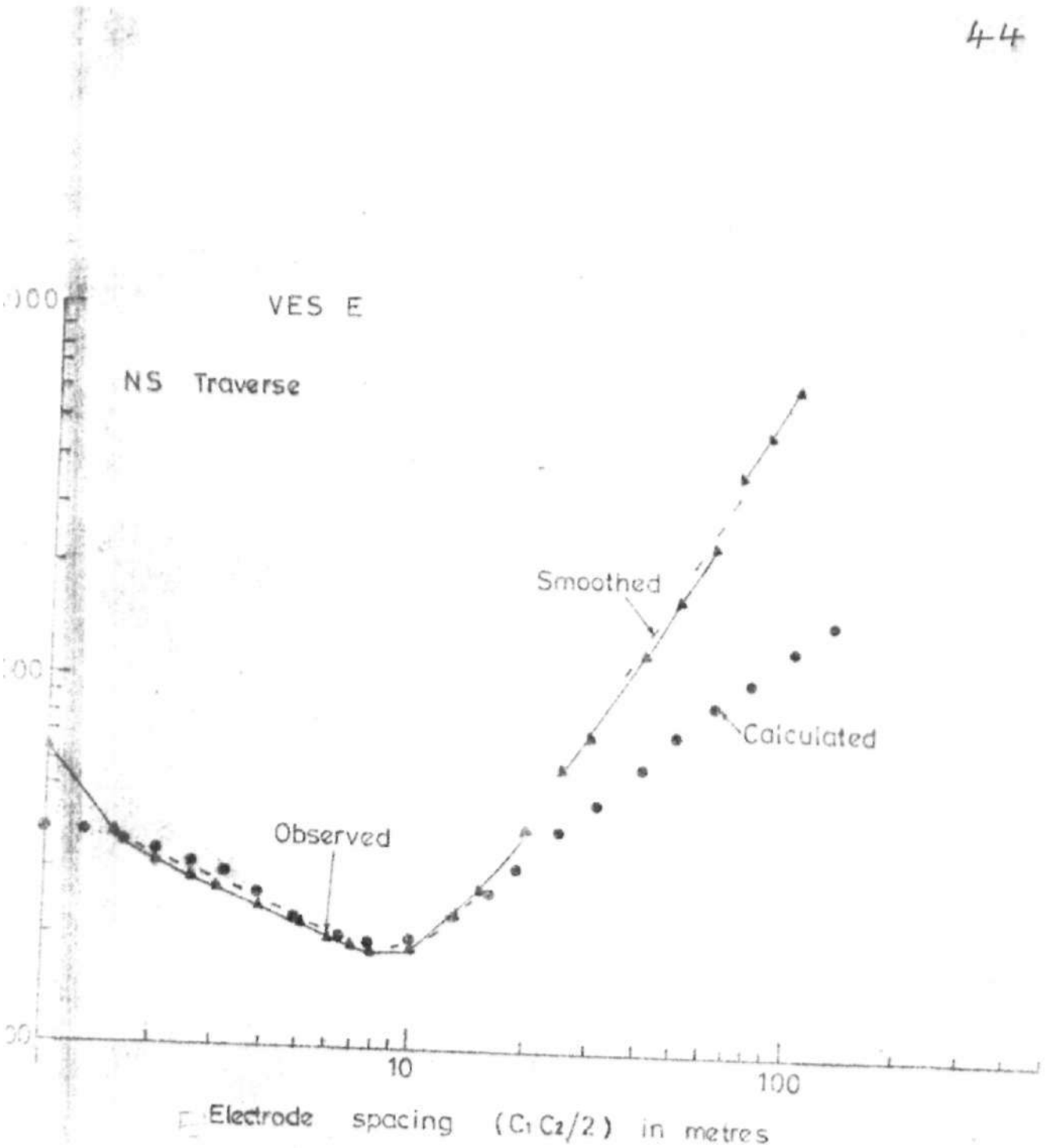


Fig. 4-8: Interpretation of VES E curves in terms of a 3-layer model.

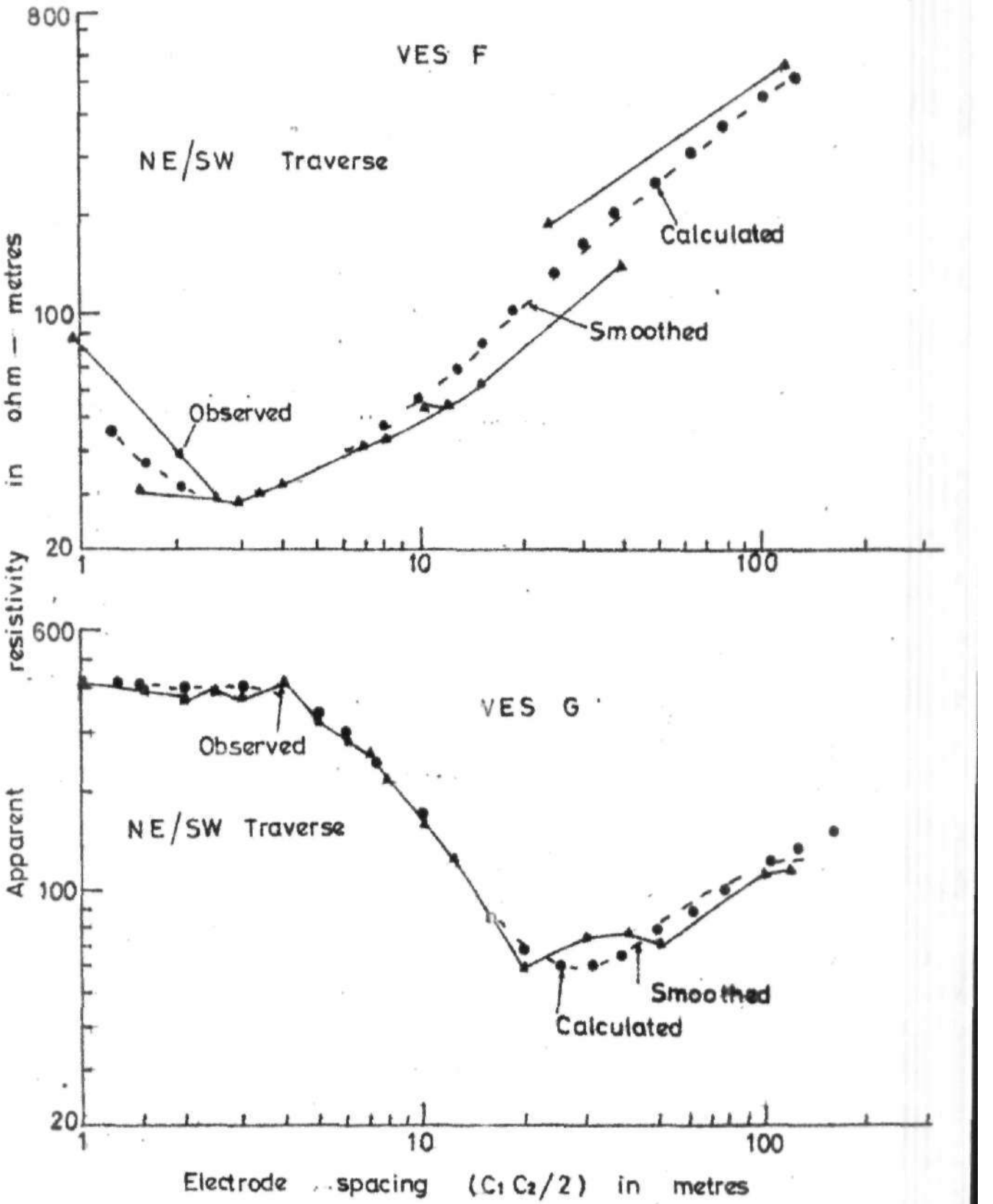


Fig. 4-9: Interpretation of VES F and VES G curves in terms of a 3-layer model.

TABLE I

Resistivities and thicknesses of geoelectric layers
(Deduced from a 3-layer interpretation)

VES	Orienta-	Layers, thicknesses (m) and resistivities (ohm-m)					Kcefored coefficient	Combined coefficient of anisotropy
		1		2		3		
		d_1	ϱ_1	d_2	ϱ_2	ϱ_3	C	λ
A	NS	1.4	360	12	53	2500	566	1.835
	EW	1.0	380	11	102	4000	431	
B	NW/SE	1.0	350	15	70	4000	857	1.634
	NE/SW	4.3	280	40	30	4000	5333	
C	NS	1.4	650	10	250	2500	100	1.773
	EW	1.2	830	10.5	156	1000	67	
D	NS	0.7	400	7.5	145	8000	414	1.133
	EW	1.0	300	12	150	5000	400	
E	NS	1.0	400	6	120	4000	200	
F	NE/SW	0.5	70	4.0	24	2000	333	
G	NE/SW	4.0	400	22.3	45	256	127	

B.

(4-layer Interpretation of VES B

		1		2		3		4
		d_1	ρ_1	d_2	ρ_2	d_3	ρ_3	ρ_4
B	NW/SE	0.85	520	3.6	165	6.5	45	4500
	NE/SW	0.80	780	7.0	180	20	13	8000

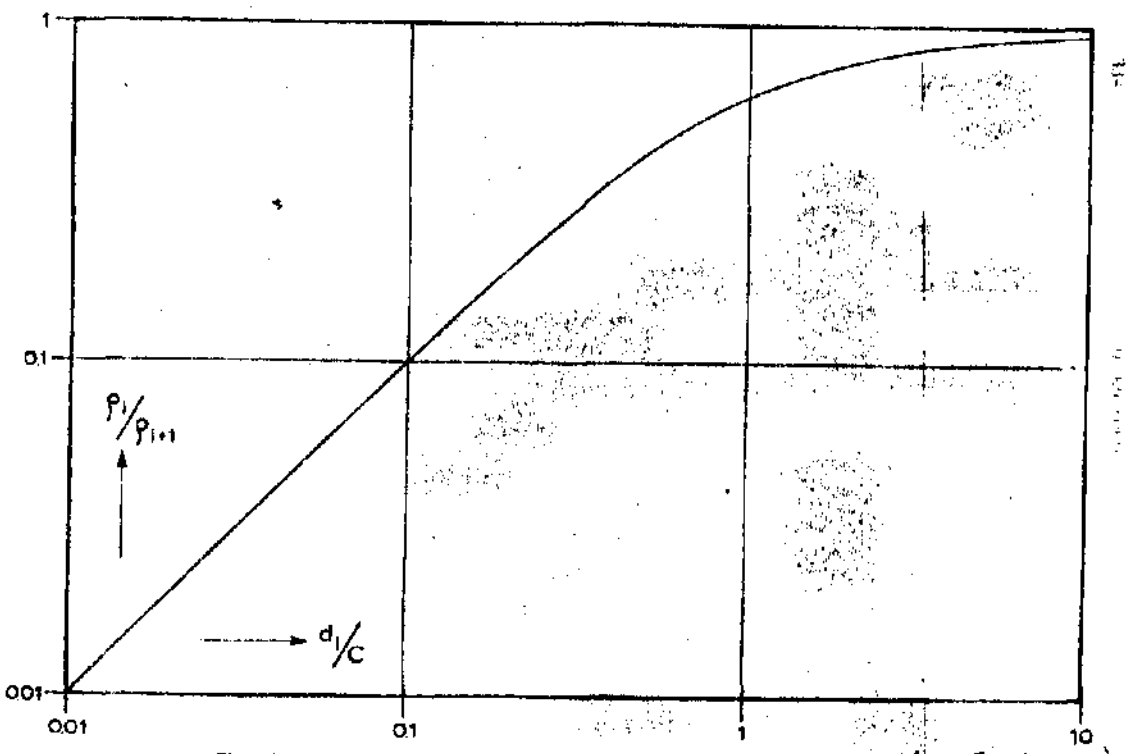


Fig. 4.10 Standard graph for the determination of equivalent cases when $\rho_1/\rho_{i+1} < 1$. (Koefoed, 1969)

The results at location E, reveal a thin surface cover of thickness 1 m and resistivity 400 ohm-m. A cross sounding would however be required to establish the accurate geoelectric section at depths.

At location F the interpretation of the Schlumberger curve indicates a surface layer of thickness 0.5 m and resistivity 70 ohm-m corresponding to a layer of micaceous clay; underlain by a kaolinitic layer of thickness 4 m and resistivity 24 ohm-m. Again to aid complete interpretation a cross sounding would be necessary.

The short-spacing data obtained with the Schlumberger array at location G suggests a surface layer of thickness 4 m, with an apparent resistivity 400 ohm-m, underlain by 22 m thick zone of low resistivity material indicative of a layer of kaolin, micaceous clay, wad and sand. The third layer of resistivity 256 ohm-m is not representative of the basement region, additional data are required to establish the situation at depth.

Discuss of Results

The simple 3-layer interpretations of the Schlumberger sounding curves show that the area is characterized by a thin overburden varying in thickness from 0.5 - 4 m. This

result in general compares favourably with the well log range of 1.2 - 4 m. The sharp rise in the apparent resistivity values observed at the various sounding points for the large current electrode spacings (10-150 m), irrespective of the electrode orientations, reflects the sporadic occurrence of the deposit. Reliable interpretation of the sounding curves by merely using the borehole log data and varying the apparent resistivities for best fits would however be masked by the irregular occurrence of the deposit and the consequent intergrading of the various rock types.

The Schlumberger sounding technique is thus incapable of yielding complete reliable quantitative measure of depths to bedrock.

4.3.2 CENTRAL ELECTRODE SOUNDING

The technique was used for exploring to various depths not exceeding 20 m at a given point. In the field measurements, 2 potential electrodes P_1 and P_2 were placed in line with the current electrode C_1 which has been placed at the point at which exploration was desired. The second electrode C_2 was placed at a far distance (300 m) from C_1 (Fig. 4.1(ii)). This method was executed only in the western section bordering boreholes 4489 and 4490 in view of the short period

available for the task.

Interpretation (Qualitative)

The apparent resistivities were calculated using the formula

$$\rho_a = 2\pi R(a'b')/(b'-a')$$

where ρ_a is the apparent resistivity; "R" the observed resistance; a' and b' are the distances C_1P_1 and C_1P_2 respectively.

The results obtained from these soundings are shown in fig 4.11. The inconsistent data obtained at location B/S may be attributed to uncertainities caused by lateral variation in resistivity. It is apparent from the two curves that the overburden is much thicker at location B/S than in location D/S. Until the course of asympotic behaviour is established the suitability of this technique is obscured.

4.3.3. SQUARE AND CROSSED SQUARE ARRAY SOUNDING

In the application of resistivity methods to the investigation of geological structures, the apparent

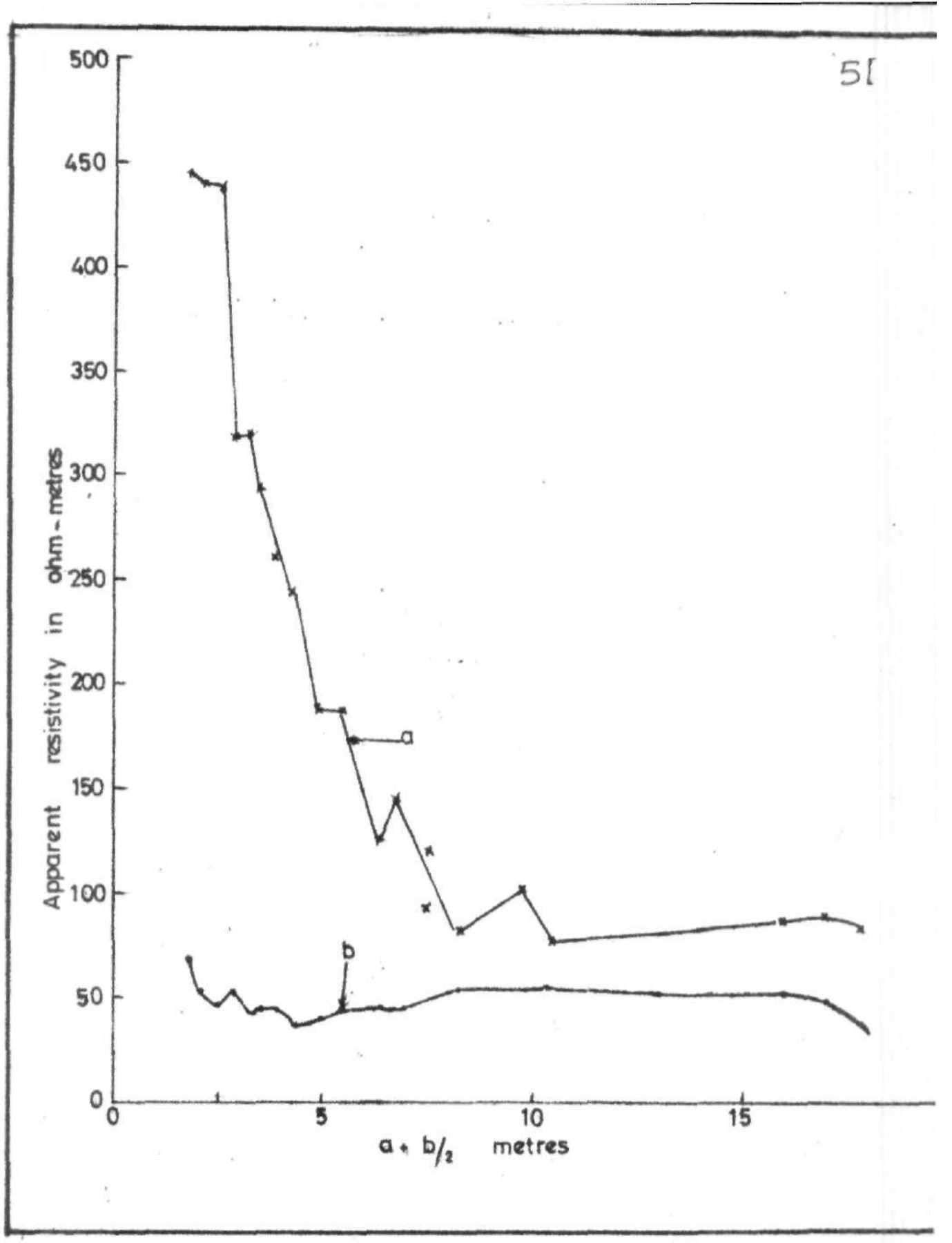


Fig. 4-11: Results of central electrode sounding at (a) location B, and (b) location D.

resistivity derived, besides depending on the electrode spacings and position of the array centre, also depends invariably on the orientation of the array.

In regions of modest dips and contrasts the square array technique which samples apparent resistivity at 2 mutually perpendicular orientations, attempts to provide apparent resistivity measure which is both more sensitive to the position of the array centre, and orientationally more stable, than the conventional collinear configurations discussed. While collinear array measurements will only reveal anisotropy as a scatter in the field results, the square array besides providing quantitative measures, also affords a check by virtue of the Azimuthal Inhomogeneity Ratio (A.I.R.) (see Appendix 1) on the existence or otherwise of orientational effects.

The square array technique would yield apparent resistivity measure that is orientationally invariant for most practical purposes as long as the maximum A.I.R. value in the measurement area does not exceed 0.2 (Habberjam 1975). In areas of severe anisotropy, the apparent resistivity however varies substantially with orientation in both the square and collinear array field systems. Under these

circumstances apparent resistivity measure deserves sampling in at least, 3 orientations. The crossed square array, which consists of two squares orientated at 45° effectuates sampling in 4 orientations. The method besides providing less orientationally dependent measure of apparent resistivity also enables apparent measures of effective anisotropy and strike to be made.

In the field operation, square soundings were executed at locations B/S and D/S (see Map 4) using the usual $\sqrt{2}$ expansion system for the electrode spacings. These locations were chosen for the following reasons: (i) the shallowest encounter (25 m) of the basement complex as contained in the borehole logs is at borehole 4490 and (ii) the thickest bulk of the kaolin mineral encountered is reported around boreholes 4489 and 4373 where the thicknesses are 14.4 m and 20.4 m respectively; and besides, the occurence of white marble in this location enhanced its prominence. The basic electrode layout for the square measurements for the N.S orientation used is shown in fig. 4.2. At each location observations were made with positions 1 and 4, 1 and 2, and 1 and 3 respectively as current electrodes.

The large A.I.R. values obtained in the above measurements (table 4.2) established that the locations were subject to large orientational effects. Accordingly, to average out these effects a second square sounding set at 45° to the square sounding originally executed at location D/S was conducted. The combined sounding thus provided data for the desired less orientationally dependent crossed square sounding.

Interpretation of Results

The field data were processed to yield mean apparent resistivities and A.I.R. values for the individual square soundings S_1, S_2 and S_3 in the areas investigated (table 4.2). The results of the square constituents S_2 and S_3 at location D/S were combined into a single crossed square analysis. From the analysis apparent values for the overall mean resistivity, anisotropy and strike were determined. The basic equations used in the processing of these data are given in the Appendix I.

Sounding at B/S

The results of the derived apparent resistivity values for this location after tripotential adjustment are plotted against the spacing used on a bilogarithmic scale (fig. 4.12).

Qualitatively, the result shows a decay from a near surface resistivity of about 200 ohm-m to a minimum of about 100 ohm-m at intermediate depth corresponding to a layer of white kaolinitic clay, mottled clay, fine grained sand and wad. Beyond this zone the apparent resistivity increases to over 200 ohm-m indicating probably the presence of basement.

Habberjam and Watkins (1967) has shown that when the mean resistivities of a square configuation of side "a" are plotted against 0.805 a or 1.207 a, rough interpretation could be made using Wenner or Schlumberger type curves. The derived equivalent schlumberger curve for this location is displayed in fig. 4.12. Interpretation was made by curve - matching procedures employing Rijkswaterkaat master curves. The quantitative analysis reveals a near surface layer, 3.8 m thick having a resistivity of 150 ohm-m, underlain by a more conductive layer (90 ohm-m)

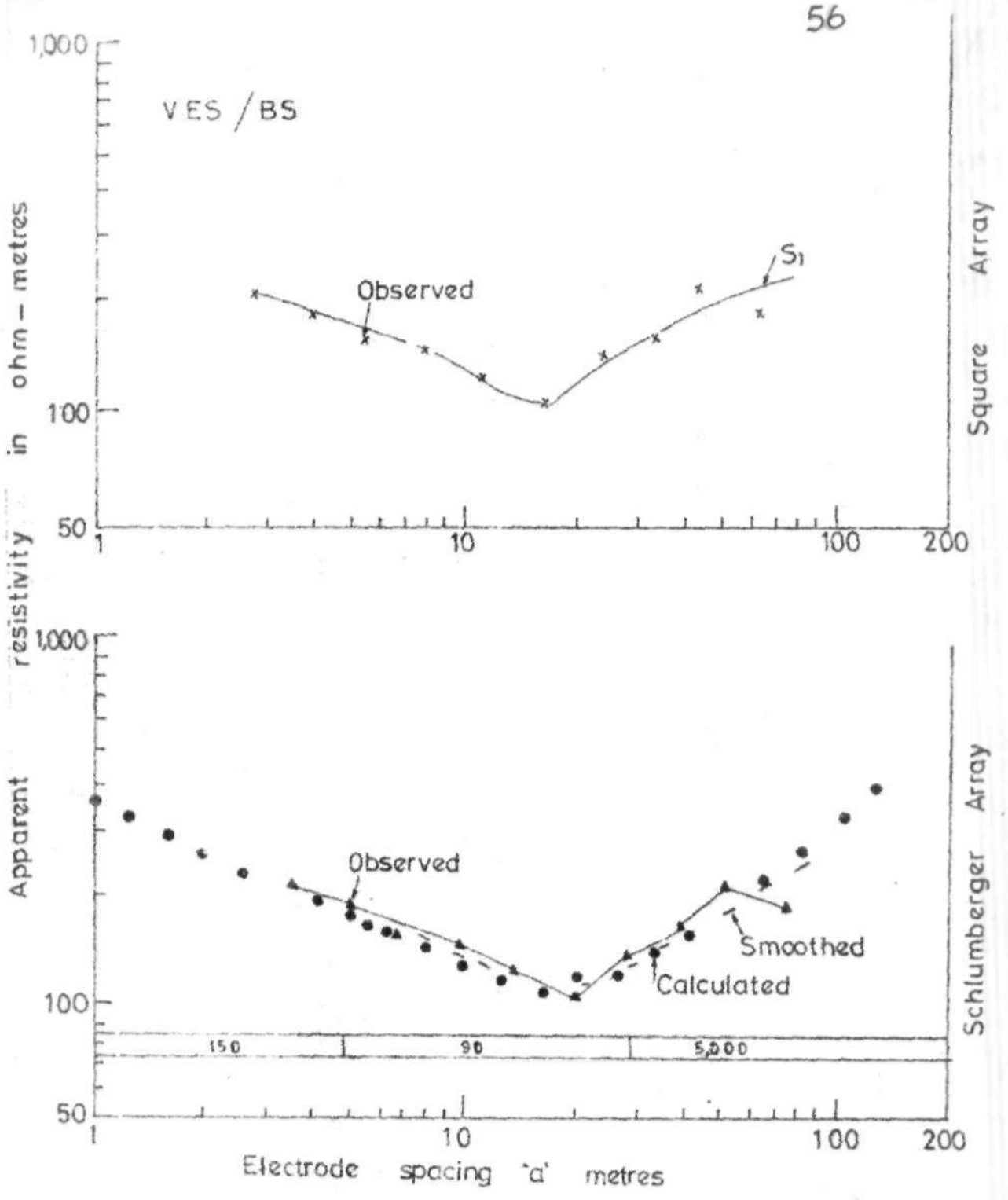


Fig. 4-12: Square array sounding results at location BS and inter- in terms of an equivalent Schlumberger sounding.

about 23 m thick. A basement resistivity of 5000 ohm-m is obtained from the analysis. Correlation of the above results with the neighbouring borehole log 4490 is quite satisfactory (fig. 4.15). The large r.m.s. A.I.R. value of 0.528 obtained for the location suggests that the discrepancy between the observed results and the borehole data is largely due to the effect of pseudoanisotropy. The accuracy of the resistance measurement 'V' which is a measure of the departure from the tripotential was found to be of an r.m.s. value of 0.122.

Sounding at D/S

The results of the two square soundings S_2 and S_3 at this location are shown in fig. 4.13. An analysis of the smoothed curve on the basis of Schlumberger type curves indicates a 5-layer set up. The thicknesses obtained from the above analysis correlates fairly well with the 4489 and 4373 borehole logs in the immediate locality (Fig. 4.15). That the location is subject to large orientational effects is confirmed by the large r.m.s. A.I.R. values of 0.732 and 0.307. These values are however not alarming in view of the prevailing heterogeneous layers, each imposing its own strike tendencies.

The anisotropically analysed detailed results of the cross sounding are embodied in table 4.2. The apparent resistivity values derived for this sounding are plotted in fig. 4.13, for comparison with the constituent square soundings S_1 and S_3. The apparent anisotropy and apparent strike are plotted against the spacing used. A scale of log (n-1) and a natural scale have been used for apparent anisotropy (n) and apparent strike (ϕ) respectively.

It is apparent from the curves of fig. 4.13 that is single square sounding does not uniquely describe the site. An interesting feature of these curves is that they all depict the same subsurface structure by virtue of their shapes. The only remarkable variations is in their apparent resistivities. This lucidly confirms the instability of the square array field system at this site. The elligibility of the crossed square sounding curve C_x as the overall mean of the square sounding curves S_2 and S_3 is clearly seen in fig 4.13. The deviation of C_x from the expected overall mean curve may be attributed to the fact that ρ_x does not depend only on the actual resistivity of the subsurface but also on the dip of anisotropy.

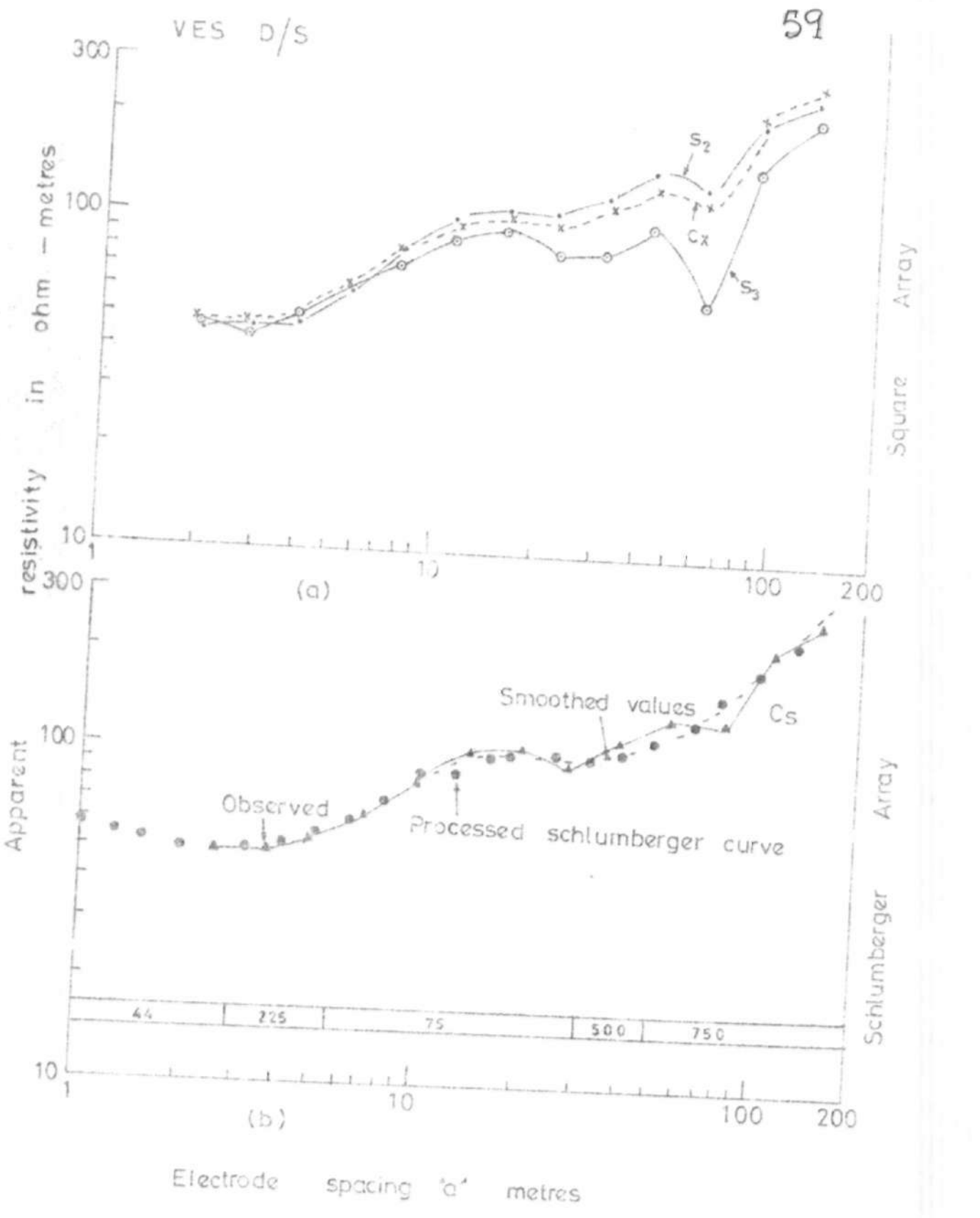


Fig. 4-13: Square and crossed square sounding results at location D/S and interpretation in terms of an equivalent Schlumberger sounding.

The apparent anisotropy varies from a minimum value of 1.02 to a maximum value of 1.51 at depth (fig. 4.14(a). From the general trend of this curve a layered interpretation could be made qualitatively of a thick and low resistivity zone over steeply dipping and relatively large anisotropic formations.

The strike of anisotropy (fig 4.14 (b))is observed to vary substantially with the spacings used. A dominant NW-SE trend (S72E) is observed for the middle layers, which accords slightly well with the approximate EW local geological strike. The discrepancy between the electrical strike and geological strike manifests the heretogeneous nature of the subsurface being examined, since these strikes can only correspond over a homogeneous anisotropic medium. At shallow depths (small spacings) the overburden imposes its own strike tendencies resulting in spurious strike variations. A sharp drop in the apparent strike direction is clearly observed in the range of electrode separation 32 - 35 m. From the borehole log this marks the seat of white marble drilled in borehole 4489. The result is reflective of the possible existence of an angular unconformity in the basement region. The above

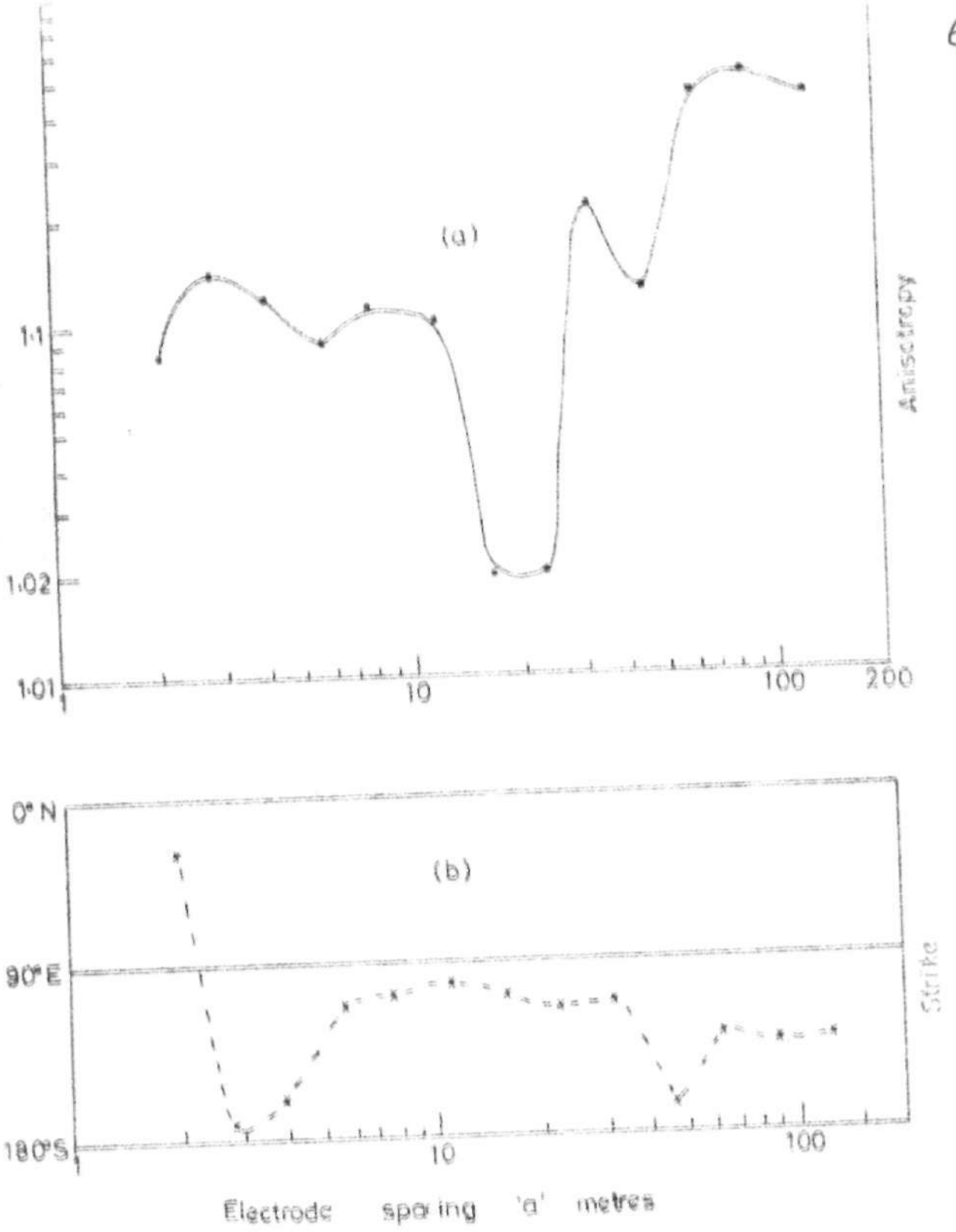


Fig. 4-14: Variations of (a) apparent anisotropy and (b) apparent strike with electrode separation.

TABLE 4.2

Results of Square (S_1, S_2 and S_3), and crossed square (Cx)
Soundings at locations B/S and D/S

Sounding		S_1	S_2	S_3	Cx	
Location		B/S	D/S	D/S	D/S	
r.m.s. A.N.C.R.	value:				0.08	
r.m.s. A.I.R.	value:	.536	.307	0.735		
Electrode spacing a_1 cm		$\bar{\rho}$ ohm-m	$\bar{\rho}$ ohm-m	$\bar{\rho}$ ohm-m	$\bar{\rho}$ ohm-m	Anisotropy n
2.0			46	47	48	1.09
2.8		209	47	45	49	1.14
4.0		186	48	54	54	1.12
5.7		156	60	66	64	1.09
8.0		150	81	74	82	1.11
11.3		127	100	90	99	1.10
16.0		106	109	94	103	1.02
22.6		138	108	81	95	1.02
32.0		161	120	82	110	1.22
45.2		216	145	99	130	1.12
64.0		189	126	58	117	1.47
90.5			213	145	222	1.51
128.0			240	212	273	1.44

interpretation is supported by the geological evidence which asserts that the marble having a NE angle of dip is discordant with the underlying SE dipping mica-schist.

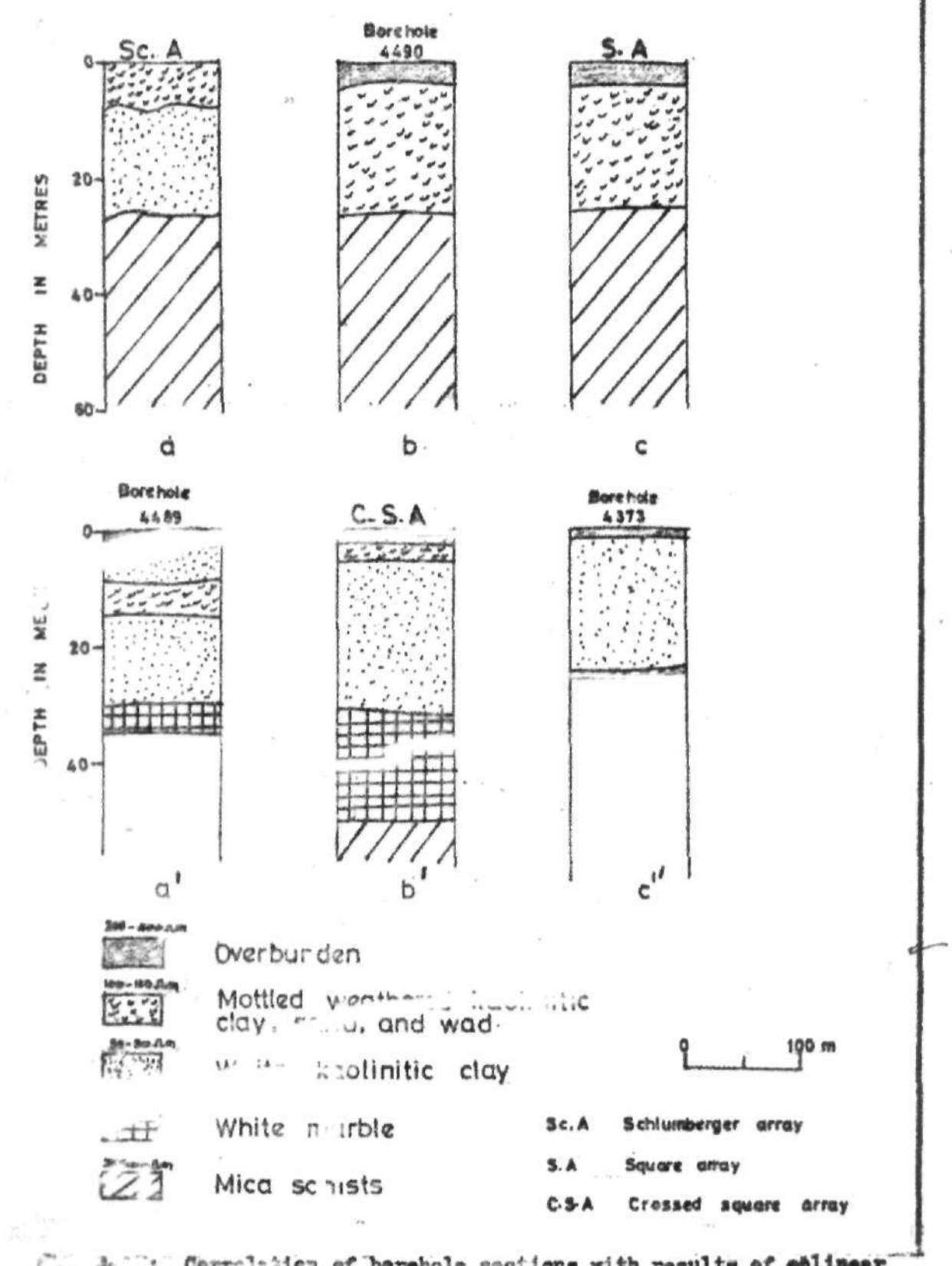
From the foregoing analyses the subsurface structure could be conclusively interpreted as consisting of a thick kaolinitic lense of a comparatively low resistivity and anisotropy bearing a predominant apparent strike S72E and being underlain by steeply dipping highly anisotropic and resistant basement rocks with no angular conformity.

The overall r.m.s. value of for the constituent square array was obtained as 0.228 and the r.m.s. value of the Anisotropic Non-compatibility Ratio (A.N.C.R) (see AppendixI) was found to be 0.080.

4.4 RESISTIVITY PROFILING

This method allows direct detection of lateral variations in the apparent resistivity values within a predetermined depth range.

In the resistivity profiling the electrode spacing used were deduced on the basis of the 7 resistivity sounding results. The Schlumberger sounding curves plotted on the field indicated generally 2 distinct points of inflection.



Correlation of borehole sections with results of collinear ... sounding.

These represent crudely the over burden - kaolinitic interface and the kaolinitic - bedrock interface. Under normal circumstances the effective depth of penetration of the current is considered roughly equal to the electrode separation for a Wenner array. Thus, by keeping the width of the array constant about these inflection points, and making a series of apparent resistivity measurements as a function of the location of the electrodes, it is possible to delineate roughly the thickness of the kaolinitic layer. This estimate is not unique, since for an inhomogenous earth the total current that penetrates a given depth is not only a function of the electrode separation but also of the resistivities of the earth layers.

The Wenner equidistant four electrode configuration (fig. 4.1) was employed in the profiling survey. Using the constant electrode separations of 5 m and 10 m derived from the schlumberger sounding results the technique was used to map out the horizontal variations in the apparent resistivity structures near the top and bottom surfaces of the kaolinitic lenses. In order to investigate the effects of deeper geologic structures constant electrode separations of 15 m and 25 m were also used. The resistivity profiling measurements were executed on 6 NW-SE, and 1 EW

traverses (map 4). The application of an NW-SE traverses, was specifically designed (1) to avoid much cutting down of trees in the struggle to clear measurement paths, and (2) to cover large ground in a single traverse measurement.

Interpretation

For each profile the apparent resistivity corresponding to the electrode separation "a" was computed from the relation

$$\rho_w = 2\pi a R \quad \text{(Wenner array)}$$

Where R is the observed resistance. The apparent resistivity values for each profile were plotted vertically against the geometric centre of the electrode configuration on a linear scale. The locations of the electrical soundings have been included on the graphs to aid in the interpretation of the profiles.

The apparent resistivity map obtained by contouring the results of each separation used is shown in Map 5. Detailed consideration for the 10 m electrode separation is given in Map 6.

Apparent Resistivity Profiles :along traverse aP

A close examination of fig. 4.16 reveals possible contact regions between a low resistivity block and a bed of much higher resistivity in the vicinity of the subsurface bordering borehole 4494. This low resistivity block correlates partially with the borehole layer of variegated kaolinitic clay. A similar but less pronounced situation is also encountered at about 125 m SE of borehole 4494. The result near borehole 4494 is in conformity with the interpretation of the VES A data which suggested the possible existence of a fault block at this location. The sharp peak observed at a distance 25 m SE of 4494 with the 25 m Wenner electrode spacing suggests that the basement might be at a higher elevation within this vicinity.

Apparent Resistivity Profile : along traverse bP

The horizontal profiling curves obtained along this profile are shown in fig. 4.17. From the systematic trends of these curves a low resistivity fault structure is apparent in the region bordering borehole 4490. This result is in fair agreement with the information supplied by the NE-SW and NW-SE VES data at this location.

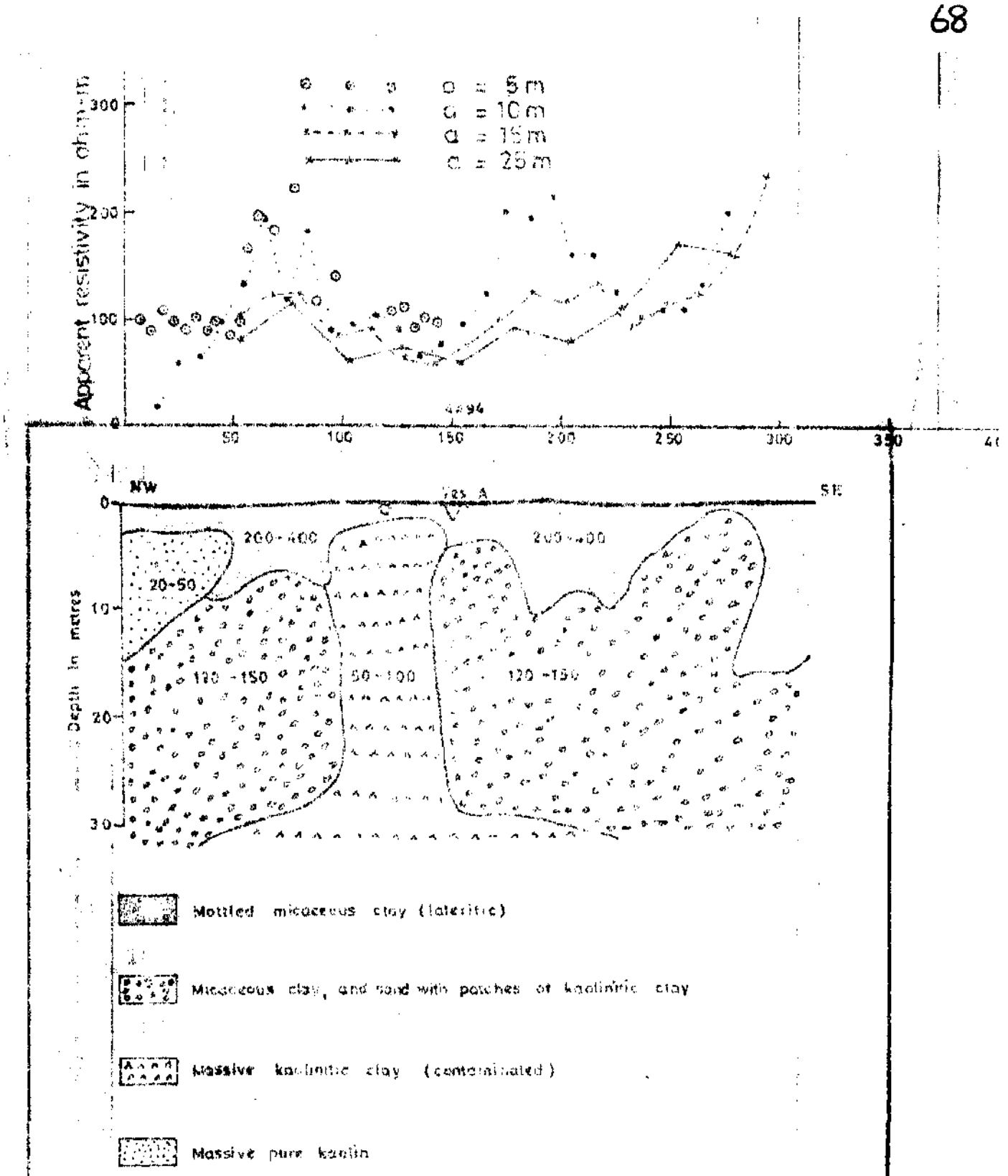
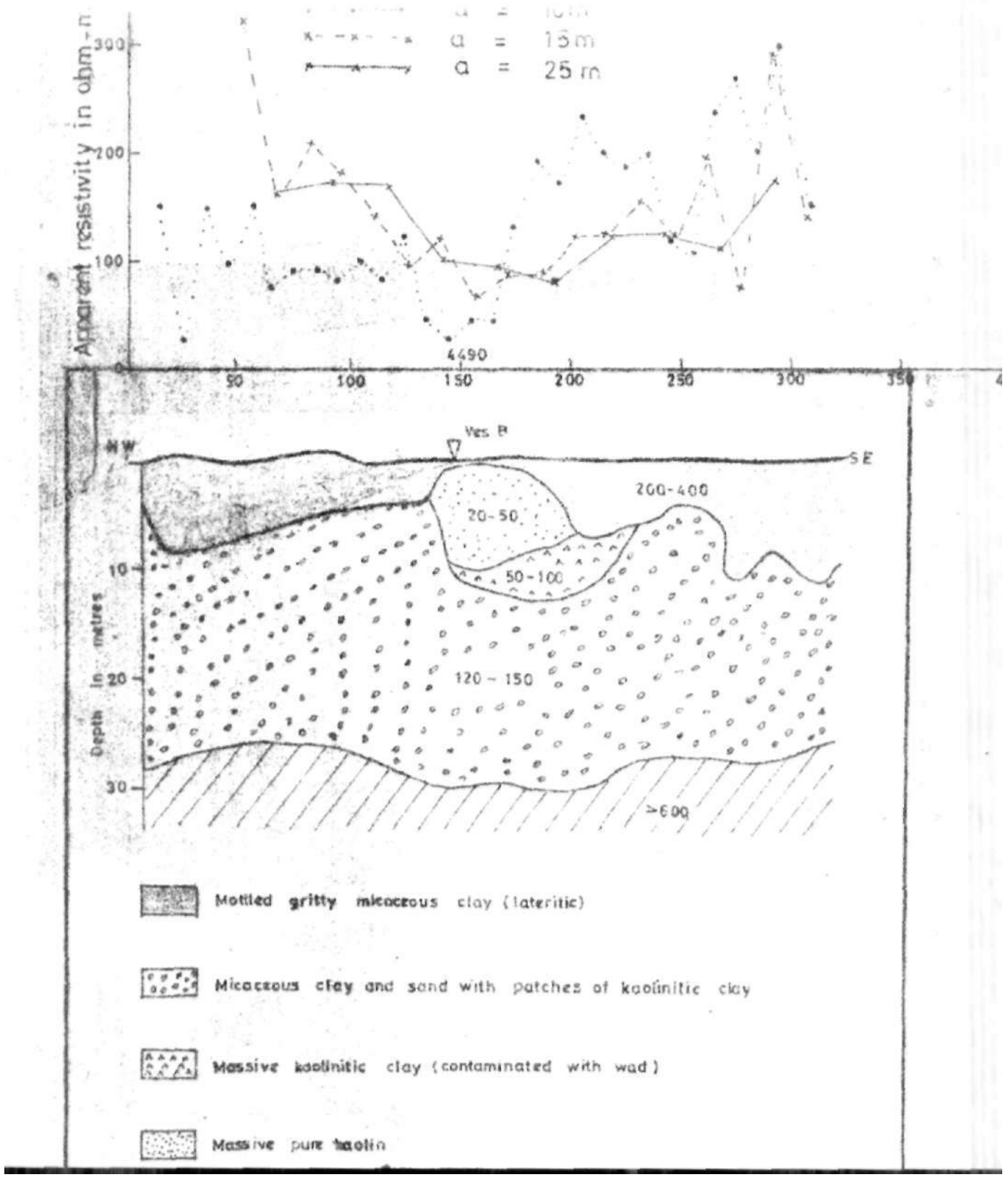


Fig. 4-16: Apparent resistivity profiles along traverse 'AB' and geological interpretation.


a = 10m
a = 15m
a = 25m
Apparent resistivity in ohm-m
300
200
100
0
4490
50
100
150
200
250
300
350
Ves 8
NW
SE
200-400
20-50
50-100
120 - 150
>600
Depth in metres
10
20
30
Mottled gritty micaceous clay (lateritic)
Micaceous clay and sand with patches of kaolinitic clay
Massive kaolinitic clay (contaminated with wad)
Massive pure kaolin

The reason for the substantial scatters in the field data obtained around the minima of both the NE-SW and NW-SE schlumberger sounding curves appear obvious from these data. These scatters manifest the contact between the bottom face of the low resistivity block and the surrounding formations as revealed in fig. 4.12.

Apparent Resistivity Profile along traverse (cP)

The observed curves and their interpretations are shown in fig. 4.18. A thick, 150-400 ohm-m resistivity cover is seen separating 2 regions of almost similar resistivities. This establishes 2 apparent resistivity troughs in the regions bordering location 4499 and an area 165 m SE of it. To probe the second layer effectively a larger current separation is required over the thick cover for both profiling and depth sounding measurements.

Apparent Resistivity Profiles along traverses (dP, cP and fP)

The results obtained along these profiles for a 10 m Wenner electrode separation are shown in figs. 4.19 and 4.20. In fig 4.20 (a) the presence of a thick overburden is indicated by the 2 well defined resistivity

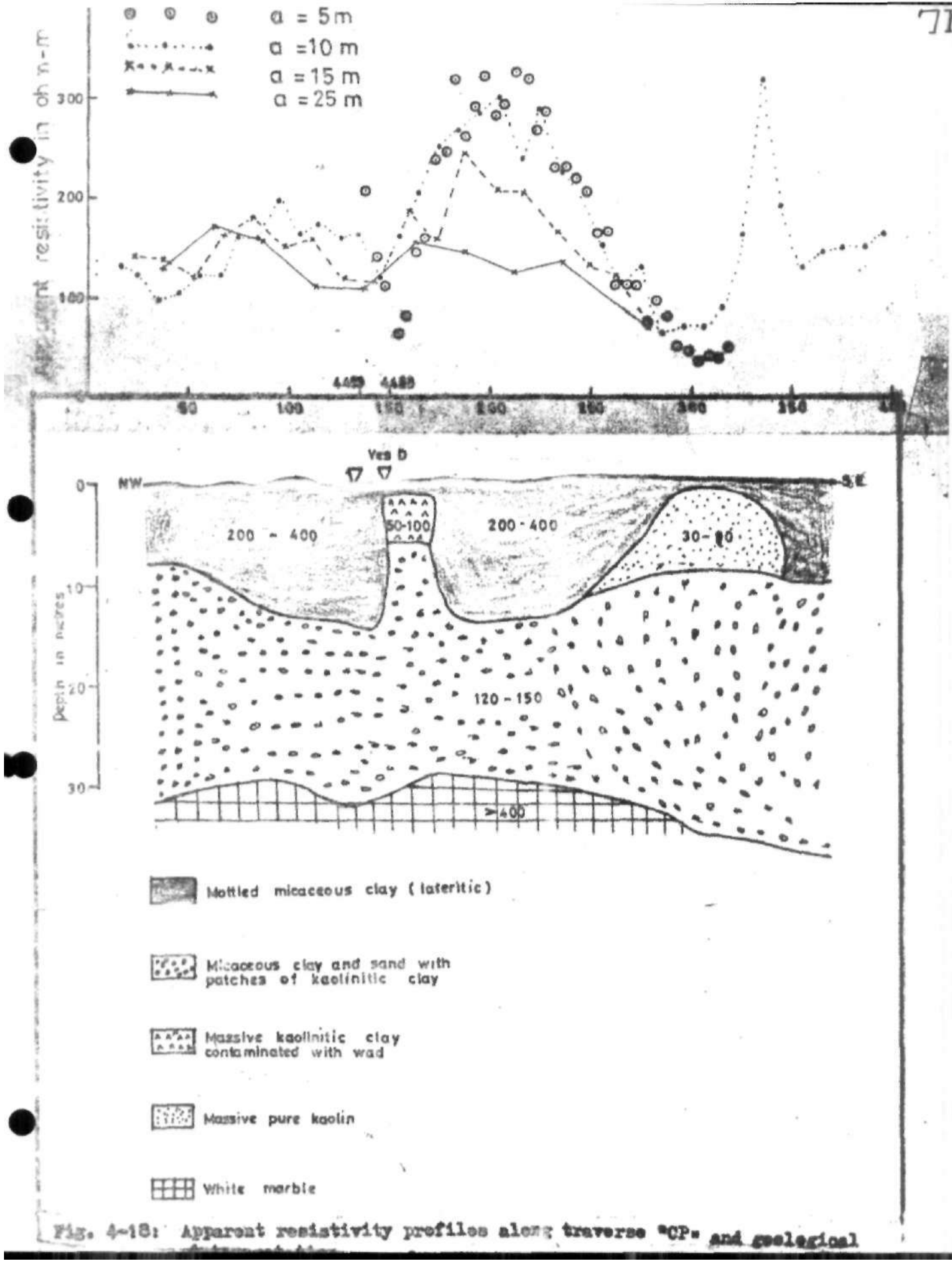


Fig. 4-18: Apparent resistivity profiles along traverse "CP" and geological

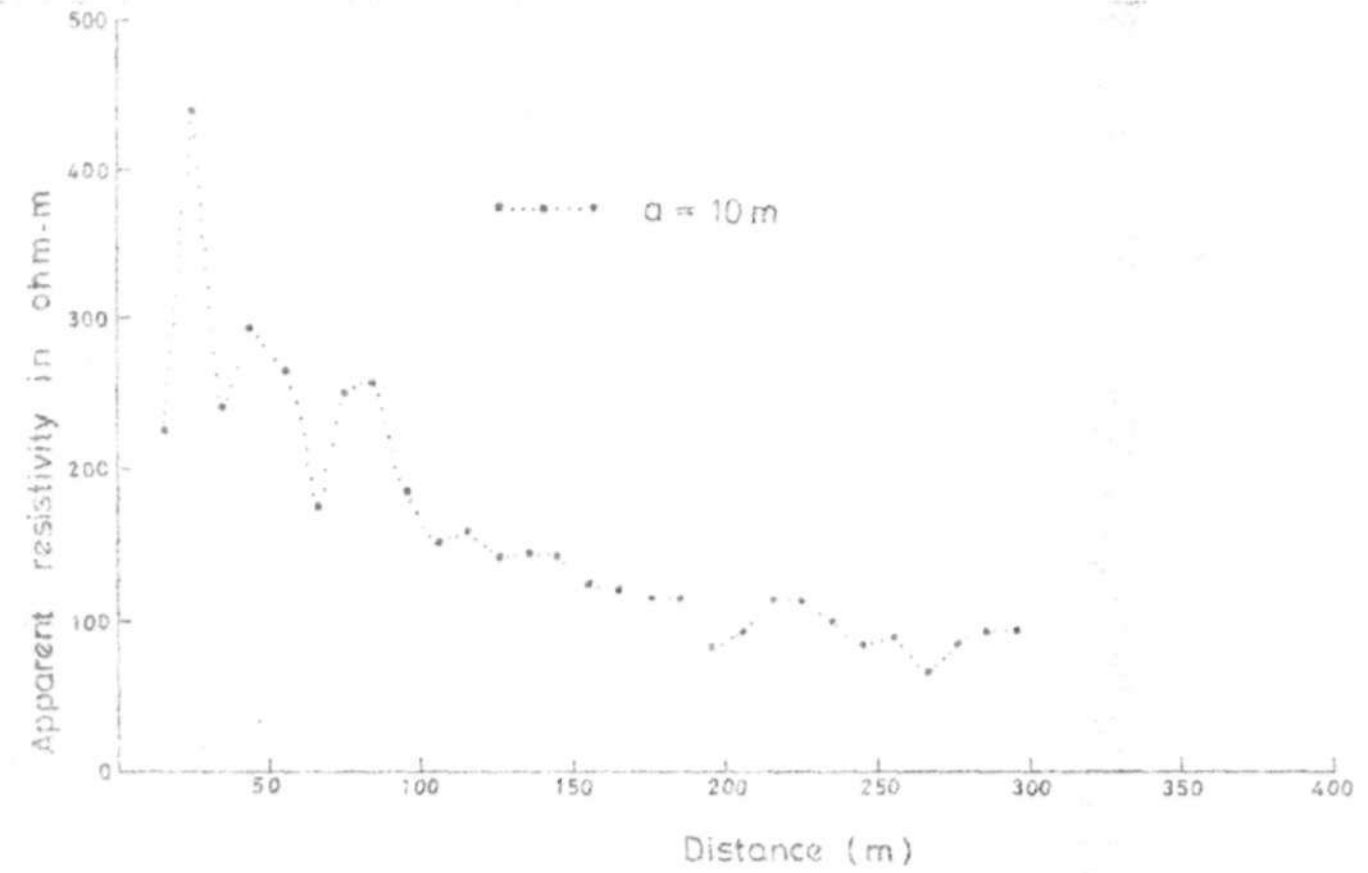


Fig. 4-19: Apparent resistivity profiles along traverse dp and geological interpretation.

troughs encountered around the 100 and 200 m station marks.

Apparent Resistivity Profile along traverse gP

The observed curves and their interpretations are shown in fig. 4.21. The VES data on this profile are inadequate to establish a true picture of the subsurface structure along this profile. However the systematic trends of both curves suggest a predominant micaceous sandy clayey layer extending well above and below the 15 m and 25 m depth ranges respectively.

General Discussion

From the foregoing analyses it is evident that the occurence of the mineral deposit is sporadic.

From the apparent resistivity map 5 the general E-W trend of the contour lines conforms with the geological evidence. In Map 6 the large resistivity contrast between the northern and southern sections of the deposit profiled by the Wenner 10-m electrode separation suggests near surface occurence of the mineralized zones in the Northern section as compared to the Southern section of the deposit. This is in conformity with the information furnished

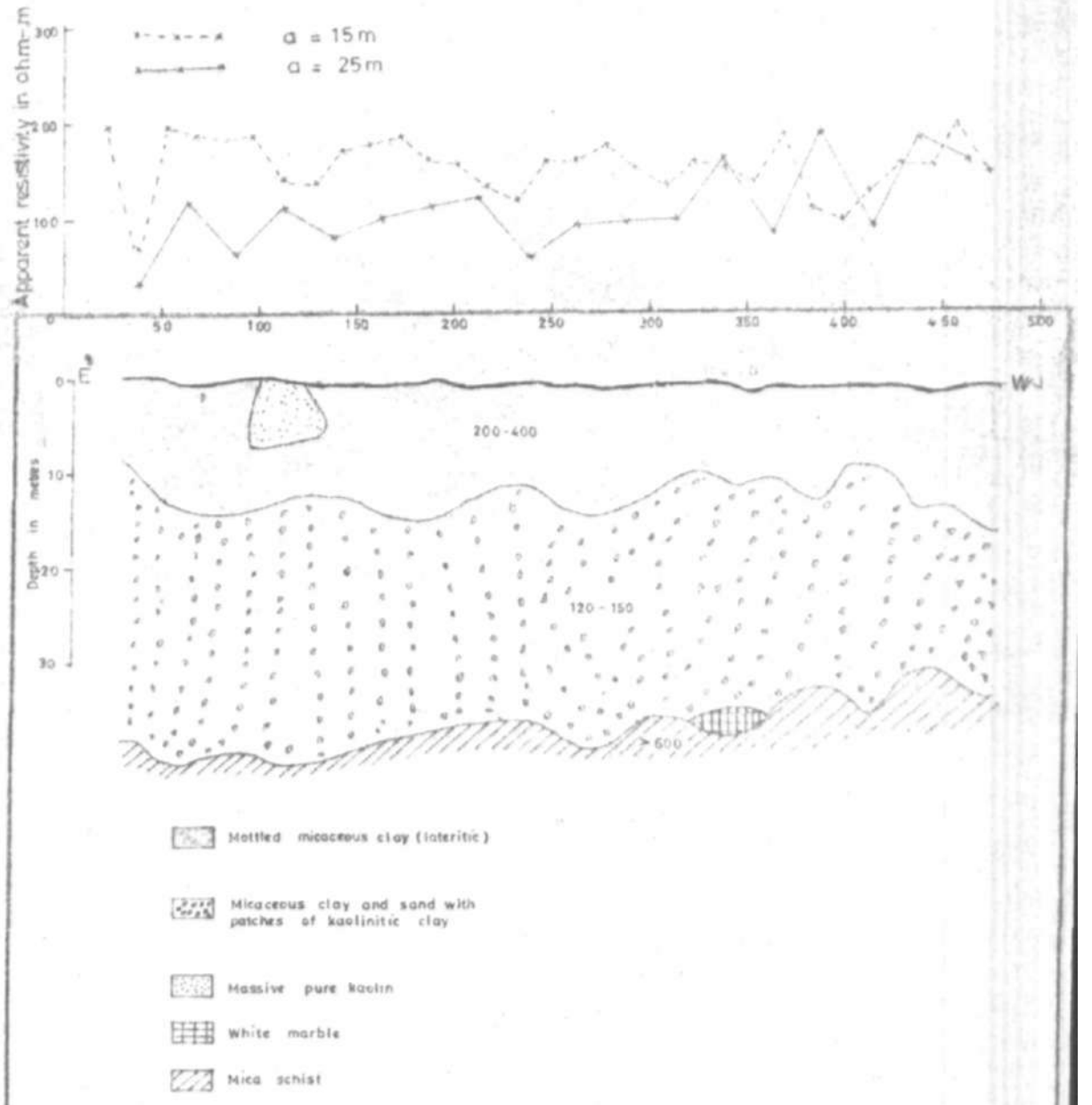
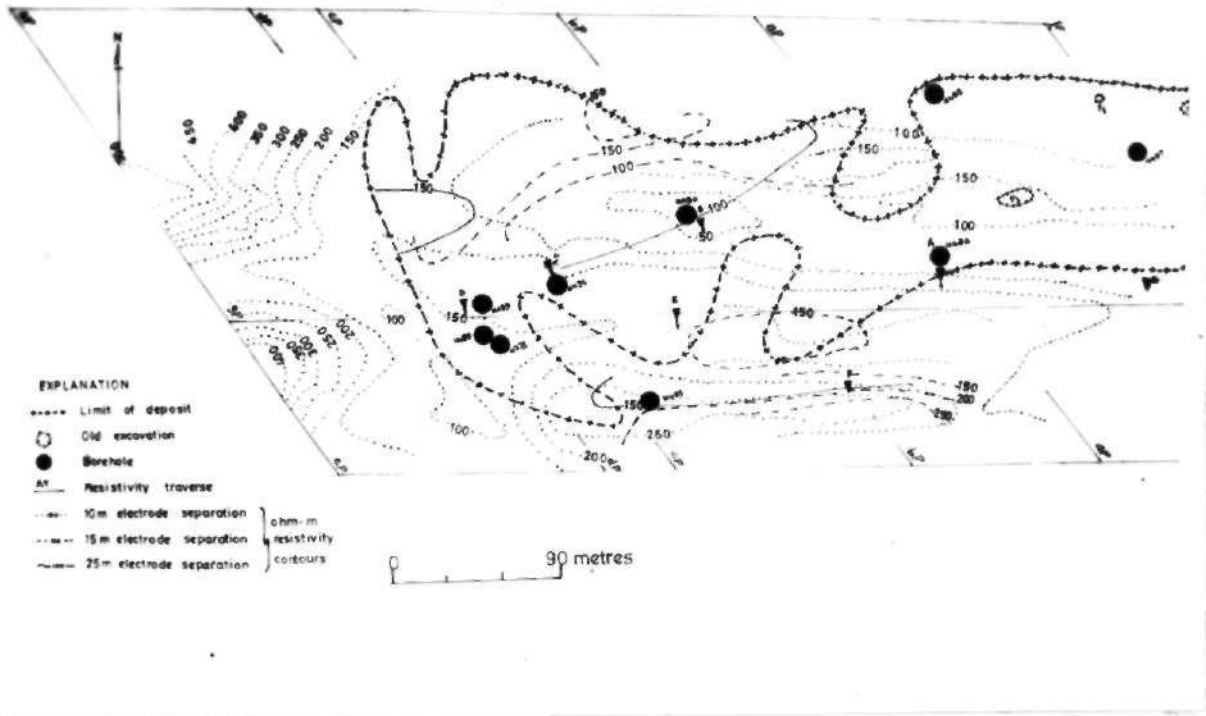
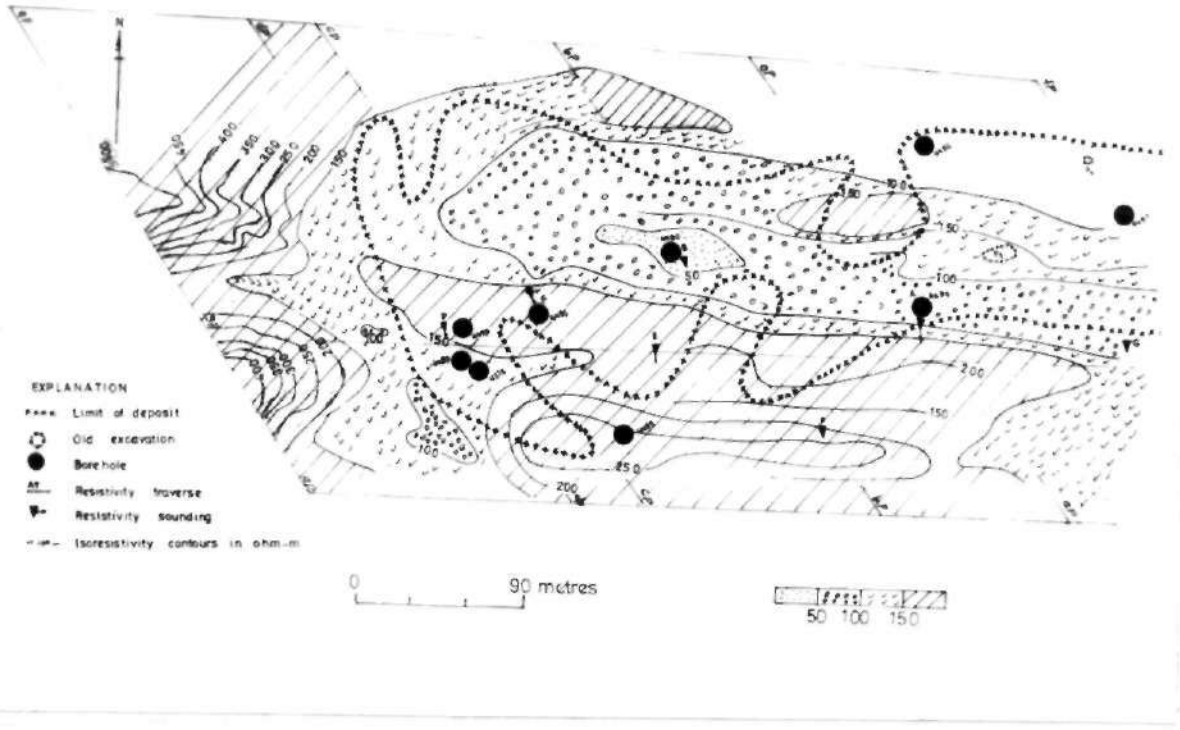


Fig. 4-21: Apparent resistivity profiles along traverse "gg" and geological interpretation.



Map 5: Apparent resistivity survey map for 10 m, 15 m, and 25 m electrode separations.



Map 6: Map of Apparent resistivity for the 10 m electrode separation.

by the borehole logs which reveal a thicker distribution of overburden towards the South. The western limit of the deposit is established by the resulting increase of apparent resistivity contrasts in this locality. A striking feature is the parallelism between the apparent resistivity contour lines marking this limit and the form of the geological boundaries.

It is apparent from the apparent resistivity profile curves of profiles bP and eP that the deposit may extend to some distance NW of bP and SE of eP.

Mass estimate of mineral body

The results of the 10 m spacing Wenner profiling show that the anomalous zone extends laterally over an area 70600 $\pm$ 1400 m^2 (Fig. 4.22). Combining this result with the results of the 5 m spacing Wenner profiling and the schlumberger geoelectric sections and using the mean density of 1.60 $\pm$ 0.18 x 10^3 kg/m^3 for the causative body; an approximate mass estimate of 5.6 $\pm$ 0.1 x 10^5 metric tons is obtained for the mineral within the horizon 5 - 10 m. The accuracy of this estimate is strongly limited by the sporadic character of the deposit and the variability of its thickness.

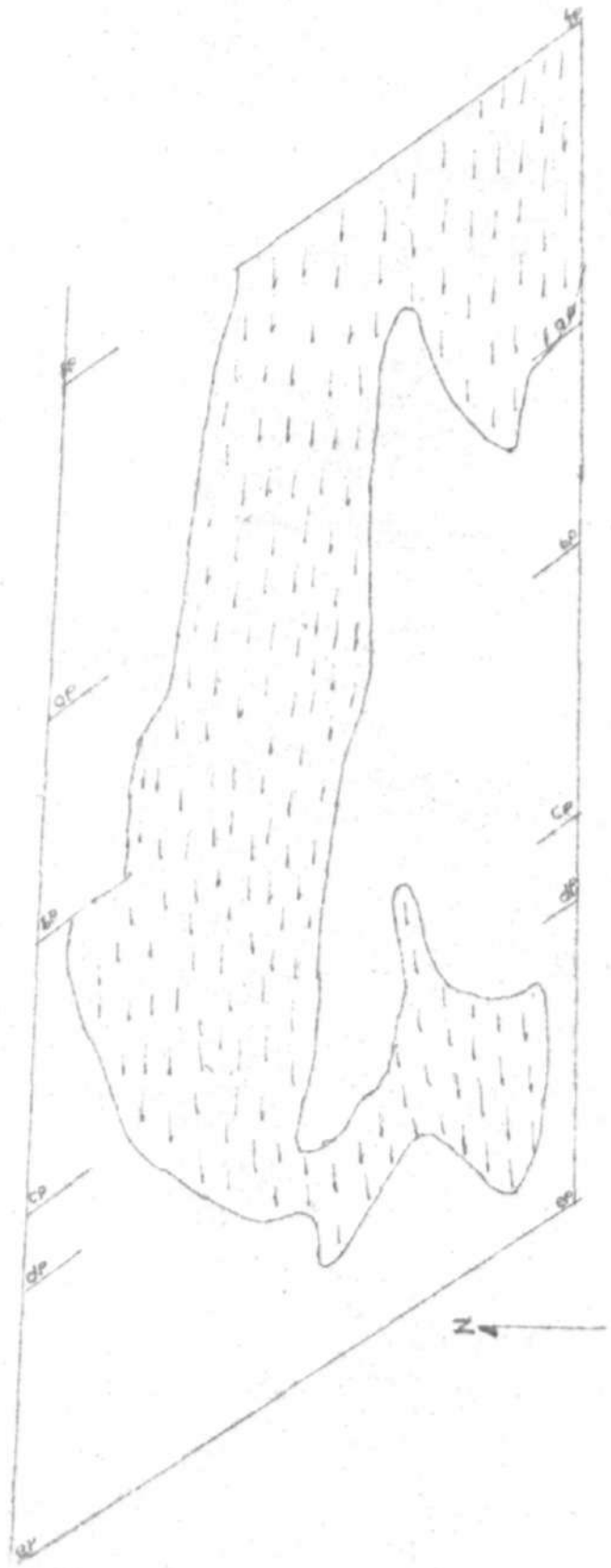


Fig. 4-22: Lateral extent of deposit derived from the 10 m interval profiling results.

CHAPTER FIVE

GRAVITY SURVEY

The method is used to map out locations of mineral lenses due to density contrast between the latter and the surrounding formations. In addition the technique enables a check on the estimates of reserves based on drilling, trenching and other mining work without the need of making any assumptions concerning the geometry and depth of the causative body.

5.1 Gravity field Methods and error evaluation

Gravity measurement were made with the Worden gravimeter (No. 135) along series of traverses covering an area of approximately 0.1 km^2. The gravimeter has a scale factor of 0.883 g.u/division and a measurement error of about 0.06% (Verheijen, Ajakaiye - in press).

The field measurements were extended beyond the anomalous zone in an attempt to obtain the requisite data for the removal of regional trends. At each station repeated observations were made until the readings differed no more than one or two units in the last

significant figure. The sequence B, D1, D2, D3, D4, B, D5, D6, D7, D8, B of measurement was adopted in the survey, where B and Di (i=1,2,3, ...) represent the reference or base station (station 00/0 in the present case) and detailed stations of the surveyed area respectively. Possible drift (gravimeter and tidal) was controlled by the re-occupation of the base station after every 2 hrs interval.

With the above procedure the maximum error in the observed gravity was estimated to be less than 0.18 g.u. An error in elevation of 0.02 m would result in an error of 0.04 g.u. in the Bouguer anomaly, The error in the instrument constant ($\pm$ 0.0005 g.u) is negligible. From the foregoing the gravity values are liable to a total absolute maximum error of 0.2 g.u.

5.2 Data Processing:

The raw gravity data were processed using the HP 9830 computer. The effects of instrument drift, elevation and Bouguer were eliminated and the convertion of the scale readings to gravity units was accomplished in the process. Terrain corrections were ignored in view of the fairly

regular ground surface, the maximum height difference encountered was about 5.0 m. over a distance of 300 m.

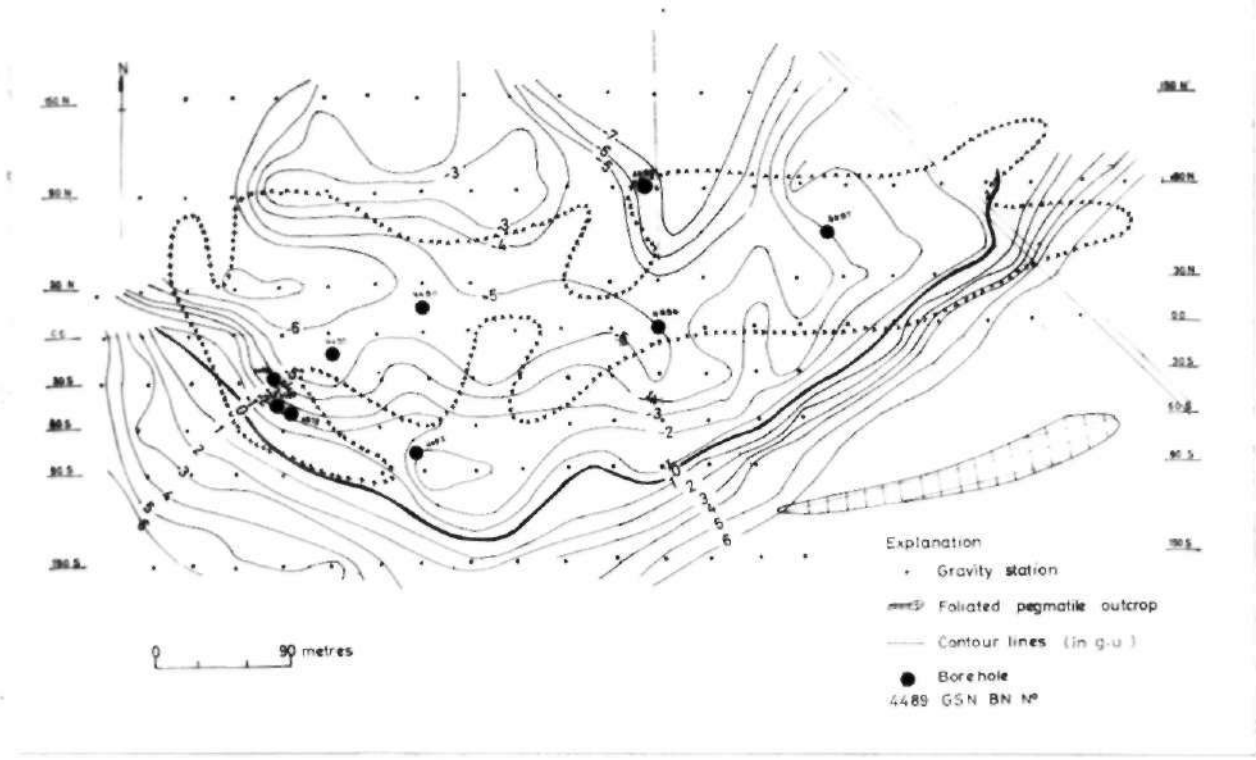
The magnitude of the regional gradient was not apparent from the initial gravity survey. A follow up regional gravity survey conducted in March 31, 1977 indicated an EW trending regional Bouguer anomaly of 5 g.u. The resulting Bouguer anomalies after the removal of the regional trends were compiled as a simple residual Bouguer contour map and profiles.

Interpretation

Gravity Contour Map

Map 7 is the residual gravity contour pattern over the surveyed area, with the regional anomaly removed.

The principal feature in the gravity map is the gravity low which evidently outlines the main core of the buried mineral. The anomalous contours in general exhibit a nosing in a direction parallel to the electrical strike which is approximately EW. The southern boundary of the concealed deposit is indicated by the positve EW trending contours closely paralleling the regional in the area. These contours are subsequently deflected upwards in the


N
Explanation
Gravity station
Foliated pegmatite outcrop
Contour lines (in g.u.)
Borehole
4489 GSN BN Nº
0
90 metres

SE boundary, marking the passing from sedimentary to igneous region.

A prominent gravity high interrupts the gravity low in the region embracing stations 90W/2W and 90N/SW suggesting either the presence of a mass of dense rock within the kaolinitic lenses or a sudden increase in the thickness of the mineral lense. The pattern of the contour at the NW side edge indicates the extension of the deposit in this direction. The occasional large gravity gradients suggests the presence of pronounced faulting in the anomalous zone.

Gravity Profiles

The Bouguer gravity profiles along traverses 150N, 30S, 00, 30S and 150S are presented in figs. 5.1 and 5.2.

Inspection of the gravity profiles reveal sections of steep gravity gradients which are suggestive of fault zones. The Bouguer gravity profile along the 00 traverse shows a valley of low density kaolinitic fills in fault contact with the adjoining rocks bordering stations 00/8W (E) and 00/0. The fault inferred in the vicinity of station 00/0 is in close agreement with the results of the

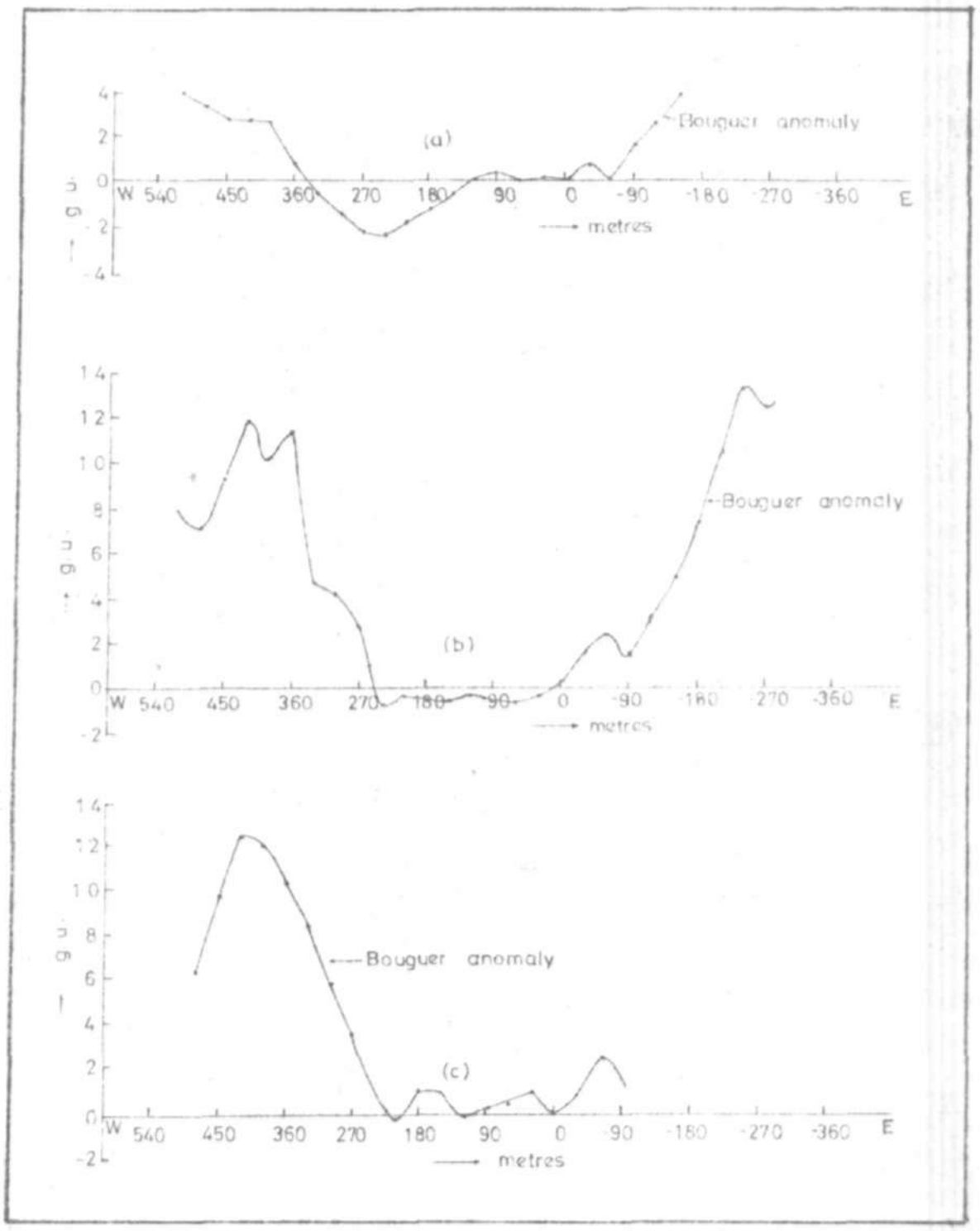


Fig. 5-1: Bouguer profiles along traverses (a) 30 N, (b) 00 and (c) 30S.

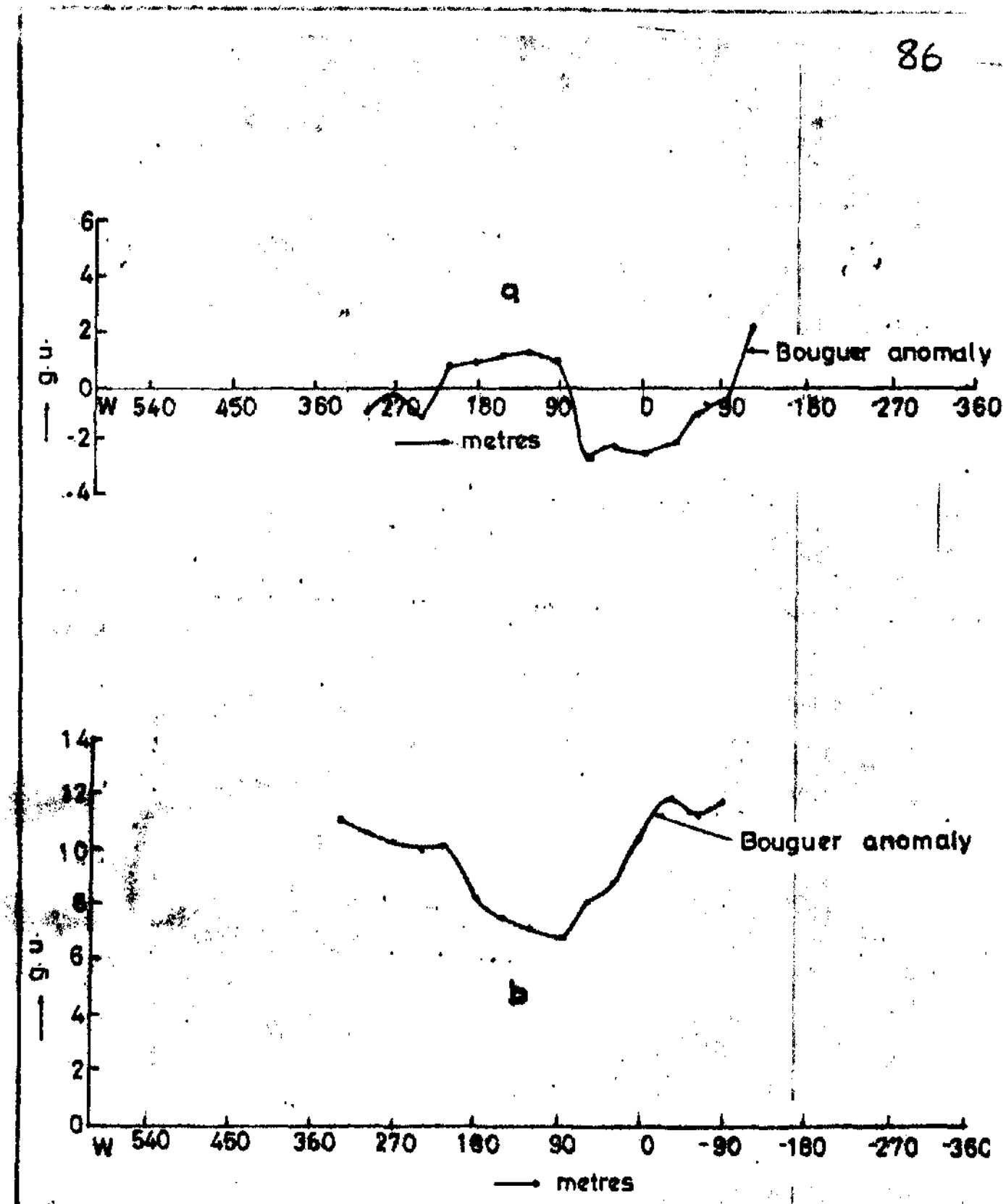


Fig. 5-2: Bouguer profiles along traverses (a) 150 N and (b) 150 E.

resistivity survey. The similarity of the Bouguer gravity profiles along the 00 and 30 S traverses suggests that the low density fills extends southwards to a distance of over 30 m. The fault zone along the 30N traverse is evidenced by the depression commencing in the vicinity of station 30N/13W .). The extreme N and S traverses 150N and 150 S show substantial variations in their Bouguer anomalies. While the result in the 150 S traverse marks the southern boundary, the need for further studies in the 150N boundary is evident.

5.4 Density Measurements

The density measurements considered in this chapter should not be confused with the initial measurements made during the preliminary analysis. The present measurements involved, 25 samples of kaolin, 10 samples of mica-Schist, and 7 samples of pegmatite.

Kaolin: Two techniques were employed in the determination of the density of the kaolin because the mineral readily disintegrates in water. In the first method the volumes of the solid mineral were estimated by the application of Archimides Principle. In the second technique the volumes

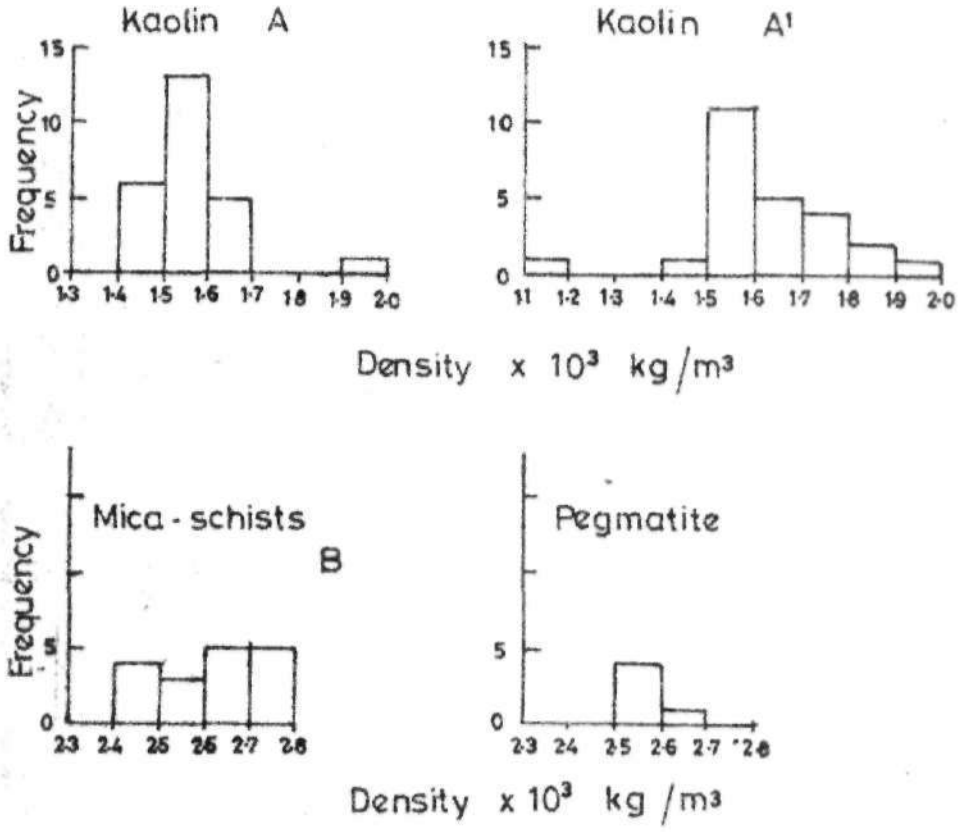


Fig. 5-3: Density histograms.

were estimated by direct calculation after the solid blocks have been shaped into rectangular blocks. The histograms for these density measurements are shown in Fig 5-3. Combining these measurements a mean density of 1.60 $\pm$ 0.18 x 10^3 kg/m^3 was obtained for kaolin.

By direct application of the Archmides Principle mean densities of 2.70 $\pm$ 0.05 x 10^3 kg/m^3 and 2.61 $\pm$ 0.03 x 10^3 kg/m^3 were obtained for the mica schist and pegmatite rock types respectively (fig. 5.3).

The densities obtained for the above rock types are much lower than expected. The reason being that most of the samples were collected from the surface and must have undergone some weathering processes. The observed densities of the kaolin (1.2 - 1.9 x 10^3 kg/m^3) are not likely to represent the densities in situ because of the rapid changes in physical states which must have taken place as the kaolin blocks were exposed to the surface. The mean value obtained however compares favourably with the mean value of 1.68 $\pm$ 0.50 x 10^3 kg/m^3 obtained by taking the mean of the relative density measurements obtained from the direct weight and volume of dry powder, and from selected

broken pieces by pycnometer, in the Geological laboratory analyses (Oyeka, 1976).

Mass Estimate

The sporadic behaviour of the causative body does not favour mass estimate in terms of definite geometry and depth. A method of mass estimation outlined in Paresins (1975) has been used in the assessment of the reserves of the deposit. The anomalous mass (Ma) is given by

$$Ma = 2.39 \sum (\Delta g \times \Delta S) \text{ metric tons}$$

Where Δg is the mean anomaly (g.u) within a small element ΔS (m^2) of the area of measurement.

The actual mass of the causatic body is given by

$$M = \rho_c Ma / \rho_c - \rho_h$$

Where ρ_c and ρ_h are the densities of the causative body and host rock - respectively.

In the present survey the anomalies outside the 0 g.u contour of the residual gravity map to a first

approximation are assumed to be zero, so that the contribution of the effectively infinite area outside it to the sum $\Sigma g \times \Delta S$ is zero. Using the above theorem and limit the anomalous mass represented by the causative body is found to be approximately $1.18 \pm 0.05 \times 10^6$ metric tons. Using densities of 1.60×10^3 and 2.76×10^3 kg/m^3 for the kaolin mineral and mica schist the actual mass of the mineral deposit is estimated to be $1.72 \pm 0.40 \times 10^6$ metric tons. This value compares fairly well with the result 1.15×10^6 metric tons obtained from the drill hole analyses.

The accuracy of the above mass estimate is however limited by (1) the possible ambiguities in the assumed anomalous boundary and (2) the influence of other clay bodies.

CHAPTER SIX

SEISMIC RETRACTION SURVEY

The method provides quantitative information about seismic velocities of various formations, depths and dips of discontinuities, due to elasticity contrast.

INSTRUMENTATION AND FIELD WORK

The seismic equipment consisted of an FS-3 portable facsimile seismograph, which is designed to record an entire seismic event initiated by an hammer impact or explosive charge on electro-sensitive paper in the form of short dashes. The hammer is equipped with a triggering device and a cable capable of covering a 60 m spread.

The survey consisted of 2 NS and 1 WE profiles derived solely from the resistivity field results (map 4). In the field operation, two geophones spaced 1 m apart were planted 0.3 m deep in the ground at one end of the spread. Impact stations were pegged along the spreads at 3 m interval from the centre of the 1 m geophone separation. Shock waves produced at each station by the hammer blow on a 0.35 x 0.03 x 0.15 m^3 steel plate, were subsequently picked

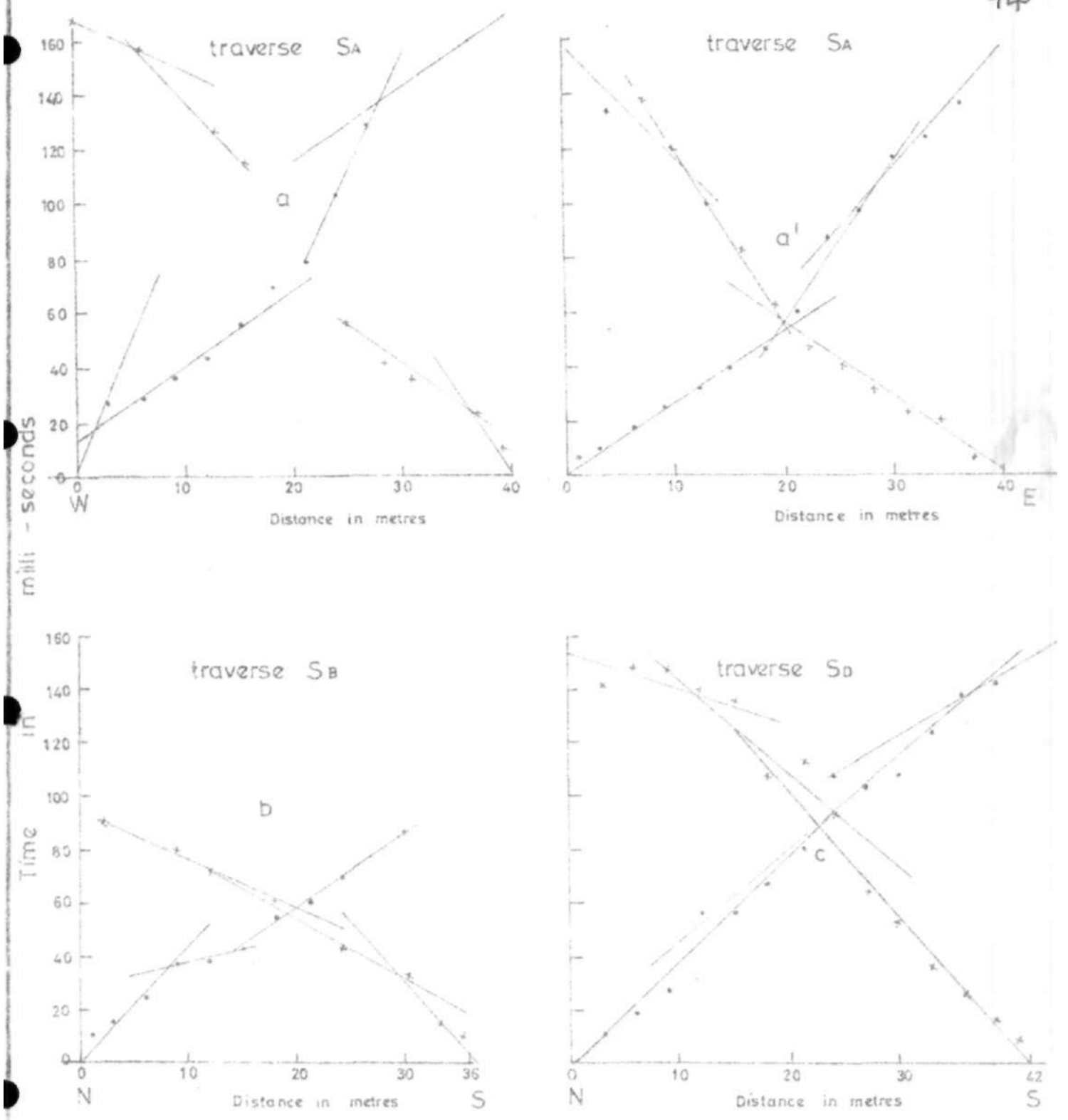
by the geophones. The travel times of the first arrivals in all cases were observed on the seismograph. At each hammer station successive traveltimes were recorded until a set of at least two values differing no more than 1 ms were obtained. The spread lengths varied from 35 m to 40 m. An error of 0.4 ms is estimated in the travel times from the seismic records. The maximum error in the slopes of the travel time curves is 12%. Error also arise from incorrect assumptions which may be attributed to velocity inversion, hidden layers and anisotropy of layered media.

Data Processing

From the seismic records, traveltime curves were plotted for both forward and reverse directions for each spread on a profile. The seismic wave velocities, dips and depths to seismic boundaries were obtained from the resulting graphs.

INTERPRETATION

The results of the seismic refraction measurement for the 2 WE, spreads along traverse SA are shown


traverse SA
a
milli - seconds
Distance in metres
W
traverse SA
a'
Distance in metres
E
traverse SB
b
Time in
N
S
traverse SD
c
N
S

graphically in fig 6.1. The velocities obtained for the first layers in spreads 1 and 2 are respectively 130 m/s and 375 m/s indicating that the near surface layers are of different rock materials. The traveltime curve "a" indicates a trend that probably reflects the buried fault intercepted in the gravity survey. The analysis shows that the distance to the trace of the fault from station 00/0 is about 18 m. The velocity of 370 m/s estimated for the second layer of spread 1 shows that this layer corresponds to the first layer of spread 2.

The traveltime graph obtained for spread 2 conforms closely with the result obtained over a vertical dike of low velocity material between two higher velocity media (Mooney, 1973).

The traveltime curve obtained for spread S_B is compatible with the results obtained over a buried vertical dike (Mooney 1973). The velocity obtained for the first layer in this NS traverse is 215 m/s with a thickness of 3.25 m, at the north end, which corresponds with the overburden thickness of 3.45 m revealed in the

borehole log 4490. The velocity of the second layer is found to be 640 m/s corresponding to a layer of kaolinitic and variegated clay, and wad. The dip at top of the second layer is found to be approximately 7.4°.

The results of spread S_D show that the tops of the second and third layers dip at angles - 1.4° and 16.2°, respectively. Velocities of 260, 283 and 483 m/s were obtained for the first, second and third layers respectively. The seismic analysis shows that the overburden has an average thickness of 7 m, underlain by a layer of approximately 5 m thick. In view of the rapid changes in soil properties within this region it is difficult to correlate the results with any of the neighbouring boreholes.

It is obvious from the foregoing analysis that seismic refraction method is capable of furnishing detail information on near surface structures. The velocities obtained for the various layers are intermediaries between dry and wet compressional seismic velocities.

CHAPTER SEVEN

GENERAL DISCUSSION OF RESULTS, CONCLUSION AND RECOMMENDATIONS

Discussion of Results

The various contributions and pitfalls of the participating geophysical methods in the delineation of the deposit are outlined below.

Resistivity: The techniques in general established the sporadic behaviour of the causative body. No definite geometric pattern could thus be associated to the body. The consequent discontinuities and orientational inconsistencies rendered the collinear arrays depth probe techniques incapable of yielding reliable measures of depths to bedrock. The major contribution of the collinear arrays depth soundings is thus limited to top layer structure, which is invariably masked by the effect of equivalence.

The square and crossed square sounding techniques which are less orientationally dependent have been particularly useful in furnishing reliable information on

depths to mineralized zones and bedrock. The results of the different sounding techniques are compared in fig. 4.15. The crossed square array also provided additional information on the variations of electrical strike and vertical anisotropy with the spacings used. The attainment of an electrical strike eventually resolved the strike paradox initially encountered on the field.

The results of the constant separation traverses using the Wenner configuration are quite satisfactory, when compared with the borehole logs. Where the boreholes did not penetrate beyond a depth of 5-10 m and in places where drilling information is lacking the resistivity profiling techniques supplied data on the existence and continuity or otherwise of the causative body. The obvious contributions of the Wenner profiling is in the delineation of the surficial and deeper body outline and location of faults and contacts.

Gravity:

Gravity measurements were useful in the mapping out of the mineralized zones, fault structures and in the assessment of the reserves. In areas where the kaolin is

contaminated there would be insuficient density contrast between the latter and other clay bodies, making the gravity method inefficient. The irregular occurrenee of the deposit would however limit the accuracy of the quantative method of interpretation.

Seismic

The method provided accurate determination of top layer structure and also assisted in the detection of near surface fault. The method was not suited to the investigation of deep seated mineral lenses and profiling of the bedrock topography.

Correlation of geophysical and geological results

In general where the various geophysical methods are applicable the results correlate satisfactorily. For example, all the three methods reveal the presence of a fault in the vicinity of station 00/0. The nosing of the residual gravity anomaly contours with a preference for the electrical strike is also a striking example.

Except for the northern and eastern extremeties where additional geophysical data are required, the correlation

between the geophysical and geological boundaries of the deposit is fairly satisfactory, particularly for the Wenner resistivity profiling. Since with the gravity methods the effects of the anomaly tail off some finite distance from the anomalous zone the marked deviation of the resulting boundary from the geological boundary is not surprising.

Comparison of the Results of the Kankara kaolin deposit with the Results of the Tsanyawa kaolin deposit

Nkuesenam (1976) conducted a similar survey near Tsanyawa, Kano State, employing basically geoelectric and seismic refraction methods. The sporadic occurrence of the Kankara kaolin deposits however limits vivid correlation between the results of the two deposits.

As a result of anisotropy, resistivity interpretations of the Tsanyawa deposit were based on data collected for current lines across the geological strike of the rocks. The analysis indicated a resistivity range of 25 - 30 m for the mineral compared to the range of 24 - 100 m obtained over the Kankara deposit. With the use of the

square and crossed square sounding techniques in the present survey the effect of anisotropy as a function of electrode spacing has been adequately assessed.

No gravity observations were made in the Tsanyawa survey, but density measurements indicated that a gravity survey would indicate a negative Bonguer anomaly in the area. The negative Bonguer anomaly values obtained in the present survey thus confirm the Tsanyawa observations.

While interpretable seismic data were obtained for spreads along the strike, in the Tsanyawa survey, the seismic data in the Kankara survey were only useful in the delin eation of top layer structure.

The magnetic susceptibility measurements over the two deposits showed that magnetic methods are not applicable. Time was not available for self-potential measurements in the present survey, but the application of this technique at Tsanyawa indicated that the method would not be appropriate.

Limitations of the Project

The wooded forest reserve, the cultivated grass land and the short period available for the execution of the project all limited the extent of the traverses used and

the spacings employed in the grid network for the gravity and other field measurements.

A major limitation to the successful application of geophysical techniques in the anomalous zone is attributed to the prevailing heterogenous nature of the subsurface. This fact is confirmed geophysically andalso by the geological evidence which asserts that "An observation of the cores obtained in the boreholes indicates that where pure white kaolin is in contact with contaminated white clay one gradually grades into the other. However where pure white clay is in contact with the altered mica-schists or otherwise pink micaceous clay there is a sharp boundary separating the two, often by fissures filled with incrustations of quartz grains", Oyeka (1976 P.4).

Conclusions:

On the basis of the evaluation described in the preceding sections, the following conclusions are obvious.

1. The Kankara 1 kaolin deposit is a valuable asset disseminated over an area of approximately 2 km^2

2. The deposit occurs in sporadic lenses and the proved reserves on the basis of the gravity result is of the order of $1.72 \pm 0.40 \times 10^6$ metric tons.
3. The deposit is subject to large orientational effects and heterogeneities and strikes electrically EW (approx).
4. The associated geophysical parameters are:-
   1. low resistivity, (24 - 100 ohm)
   2. relatively low density ($1.5 - 1.91 \times 10^3$ kg/m^3)
   3. low magnetic susceptibility ($6 - 8 \times 10^{-5}$ S. I units)
   4. apparent vertical anisotropy varying between 1.02 - 1.51

Recommendation for Future Geophysical Work:

It is recommended that further geophysical studies be carried out to determine the extension or otherwise of the deposit in the northern extremeties bordering traverse 150N.

The following procedure should be adopted when investigating the present site or a new site by geophysical prospecting methods.

(a) The area should first be covered by a detailed gravity survey at short grid spacings (say, 5 m, square grid).

(b) The thickness of the surface layers of interest should be established by a comprehensive crossed square sounding technique. The area should on the basis of the sounding result be traversed, using preferably the square configuration technique outlined by Habberjam and Watkins (1967 pp 450); in which for a W - E traverse measurement, the centre of the square array of constant side "a" is moved successively from W to E in increments of a, measurements being taken with current flow to N, E and NE respectively according to the Scheme shown in fig. 4.2

Note: On the basis of the electrical strike derived from the analyses of 2 or 3 crossed square soundings, the collinear configurations of sounding and mapping could be effectively utilized. Crossed linear soundings, along and across the electrical strike

should be performed. The overlap technique of Wenner profiling should be preferably used.

(c) The Seismic refraction measurements could then be applied as a check on the depths to top layer and bedrock (where possible) as determined by the sounding results.

REFERENCES

Ajibade, A. C.: Provisional classification and Correlation of the Schist Belts in North-Western Nigeria, Geology of Nigeria, Kogbe (ed.) Elizabethan Publishing Co., Lagos, Nigeria, PP. 85 - 90, 1976.

Bhattacharya, P. K.; and H. P. Patra: Direct current Geoelectric Sounding, Methods in Geochemistry and Geophysics, Elsevier Publishing Co., New York, 1968.

Daley, R. A.; G. E. Manager and S. D. Clerk (Jnr): "Densities of Rocks", Handbook of Physical constants, Clerk (ed.) Geol. Soc. Am. Mem. 97, New York 1966.

Dobrin, M. B.: Introduction to Geophysical Prospecting, McGraw Hill Book Company, 1976.

Evershed & Vignoles Ltd.: A pocket book on Resistivity Prospecting with Megger. Earth Testers.

Habberjam, G. M.: Effects of anisotropy on square array resistivity measurements, Geophysical Prospecting Vol. 20 Pp 249 - 266, 1972; Apparent Resistivity, Anisotrop tropy and strike measurements, Geophysical Prospecting, Vol. 23, No. 2, Pp 221 - 247, 1975.

Habberjam, G. M. and G. E. Watkins: The use of a square configuration in resistivity Prospecting, Geophysical Prospecting, Vol. 15, Pp 445 - 467, 1967.

Huntec (70) Ltd: Operators manual for the portable Facsimile seismograph; Manual of Fs-3 Seismograph Ser. No. 144, Toronto.

Johnstone, S. J. and M. G. Johnstone: Minerals for the chemical and Allied Industries, Chapman and Hall, London, 1961.

Keller, G. V.: Electrical properties of Rocks and Minerals, Handbook of Phy. Const. Clark, (ed.) Geol. Soc, Am. 97, New York Pp. 553 - 578, 1966.

Kirsch, H.: Applied Mineralogy for Engineers, Technologists and students, Chapman and Hall, London, 1968.

Koefoed, O.: An analysis of Equivalence in resistivity Sounding, 1969.

Kreiter, V. M.: Geological Prospecting and Exploration, MIR Publishers Moscow, 1968.

Kunetz, G.: Principles of Direct Current Resistivity Prospecting, Geo-publication Associates Berlin-Nikolassee, 1966.

Macleod, W.: Kaolin Deposits near Bichi, Kano Province and near Kankara, Katsina Province, Geol. Surv. Nigeria Unpub. Rept. No. 1442.

Mooney, H. M. (ed.): "handbook of Engineering Geophysics, Bison Instruments Inc. Minnesota, 1973.

Nkuesenam, O. E.: Investigation of the extent of kaolin deposit near Tsanyawa, Kano State Nigeria, using Geo-electrical, and Seismic Refraction methods, M.Sc. thesis, Dept. of Physics, Ahmadu Bello University, Zaria, Nigeria, 1976.

Oyeka, A. N.; Report on Kankara kaolin deposits, Kankara, Katsina Province, North central State with notes on marble occurence, Geol. Surv. Nigeria unpub. Rept. No. 1529, 1976.

Parasnis, D. S.: Principles of Applied Geophysics, Chapman and Hall London, 1962; Mining Geophysics, methods in Geochemistry and Geophysics 3, Elsevier Scientific Publishing Co. London, 1973.

Press, F.: Seismic Velocities, Handbook of Physical constants, Clark (ed.), Geol. Soc. Am. Mem. 97, New York, Pp. 195 - 218, 1966.

Rijkswaterstaat: Standard Graphs for Resistivity Prospecting, European. Association of Exploration, Geophysicists Netherlands, 1966.

Waudby - Smith, J. D.: A summary of the Principal known deposits of clay in Nigeria, Geol. Surv. Nigeria unpub. Rept. No. 1395.

Whyte, W. S.: Basic Metric surveying, Butterworth and Co., Ltd., London 1971.

Zohdy, A. A. R.; C. P. Eaton: Techniques of Water - Resources Investigations of the United States Geological Survey. "Application of Surface Geophysics to Ground-water investigations Book. 2, Chapter DI U. S., Govt. Printing Office, Washington, 1974.

APPENDIX I

The anisotropic analysis of square and crossed square array measurements

Apparent Anisotropy

In surface resistivity measurements where the bedding planes are dipping at an angle α, the effective vertical anisotropy n is given by

$$n = (1 + (\lambda^2 - 1)\sin^2 \alpha)^{\frac{1}{2}}$$

In this expression λ is the dimensionless anisotropy ratio defined by $\lambda = \sqrt{\rho_t / \rho_l}$ where ρ_t and ρ_l are the resistivities perpendicular to and parallel to, the bedding respectively. The anisotropy n varies between a value of 1 when the dip is horizontal and λ when the dip is vertical. The situation where λ is greater than 1 (prolate anisotropy) is that commonly encountered in stratified material, as opposed to the case where λ is less than 1 (oblate anisotropy). In practice, the anisotropy controls the effective resistivity and thickness of a layer.

Square Array Soundings (Harberjam 1975)

For a given square configuration the isotropically defined mean apparent resistivity and the Azimulthal inhomogeneity

Ratio (A.I.R.) are given respectively as

$$\rho(i) = \prod a_i \, (R_\alpha(i) + R_B(i)) / (2 - \sqrt{2})$$

$$A.I.R = 2R_Y(i) / (R_\alpha(i) + R_B(i))$$

Where $R_\alpha(i)$, $R_B(i)$ and $R_y(i)$ are the observed resistances corresponding to current flow through the 1 and 4, 1 and 2, and then 1 and 3 electrodes respectively for the i th square. These 3 resistance measurements are subject to the tripotential condition.

$$R_\alpha(i) = R_B(i) + R_y(i)$$

The tripotential ratio ν, which stems from apparent departures from the tripotential rule and attributed to errors in restance measurement is given for any constituent square array as

$$\nu = (R_\alpha(i) - R_\beta(i) - R_y(i) / (R_\alpha(i) + R_\beta(i) + R_y(i))$$

Crossed Square Array

It has been demonstrated (Habberjam 1975) that at the surface of a uniform and prolately or oblately anisotropic half space, the apparent strike ϕ, the mean resistivity ρ_m and the effective or apparent anisotropy n, determined

from crossed square resistance measurements are given respectively by

$$\tan 2\phi = (D^{-2} - C^{-2}) / (A^{-2} - B^{-2})$$

$$\rho m = 2na\,(t - s)^{-\frac{1}{2}}$$

$$n = ((t + s) / (t - s))^{\frac{1}{2}}$$

Where $t = A^{-2} + B^{-2} + C^{-2} + D^{-2}$ and

$$s = 2\,((A^{-2} - B^{-2})^2 + (D^{-2} - (^{-2})^2)^{\frac{1}{2}}$$

The constant A, B, C and D are expressed in terms of the configuration resistances as

$$A = 3R_1/2 + R_2/\sqrt{2} + R_3/2 + R_4/\sqrt{2}$$

$$B = R_1/2 + R_2/\sqrt{2} + 3R_3/2 + R_4/\sqrt{2}$$

$$C = R_1\sqrt{2} + 3R_2\sqrt{2} + R_3/\sqrt{2} + R_4/2$$

$$D = R_1/\sqrt{2} + R/2 + R_3/\sqrt{2} + 3R_4/2$$

Where R_1, R_2, R_3, and R_4, have been used in the place of R_α, R'_α, R_β, and R'_β respectively (see fig 4.2)

The Anisotropic Non - compatibility Ration (A.N.C.R) which conceptually plays a similar role to that of A.I.R. in the square array is given by the expression.

$$\xi = E / t$$

Where $E = A^{-2} + B^{-2} - C^{-2} - D^{-2}$ represents a failure of the derived resistance values A, B, C and D to conform with the requirements of uniform anisotropy.

Where $E = A^{-2} + B^{-2} - C^{-2} - D^{-2}$ represents a failure of the derived resistance values A, B, C, and D to conform with the requirements of uniform anisotropy.

Where $E = A^{-2} + B^{-2} - C^{-2} - D^{-2}$ represents a failure of the derived resistance values A, B, C, and D to conform with the requirements of uniform anisotropy.